Raquel Mier González

APPLICABILITY OF POLYMER-CERAMIC COMPOSITE COATINGS TO REPAIR METAL COMPONENTS

Thesis
CENTRIA UNIVERSITY OF APPLIED SCIENCES
Industrial Management
June 2020

Centria
UNIVERSITY OF APPLIED SCIENCES

ABSTRACT

Centria University of Applied Sciences	Date	Author
	June 2020	Raquel Mier González

Degree programme
Industrial Management

Name of thesis
APPLICABILITY OF POLYMER-CERAMIC COMPOSITE COATINGS TO REPAIR METAL COMPONENTS

Instructor	Pages
Jonne Näkki	61

Supervisor
Jonne Näkki

The aim of this thesis was to study the applicability of polymer-ceramic composite coatings to replace metallic coatings in repairing of metal components. In the literature part, previous studies about composites consisting of a polymer matrix reinforced with micro-sized ceramic particles were reviewed. However, few studies were found and it seemed that these studies handled a wear type or an environment different from this study. This study focused on coatings reinforced with particles larger than 1 mm, which are used in the harshest wear environments.

In the experimental part of this thesis, different commercial epoxy-ceramic composite coatings (Belzona 1811, ARC MX1 and ARC BX2) and an unreinforced polyurethane coating (Belzona 2121) were examined. A pull-off test was performed using a Positest AT-A Automatic device to measure the adhesion strength of these coatings to the substrate. The abrasive wear resistance was measured with a Taber abraser and the erosive wear resistance was measured with a high-speed slurry-pot type erosion tester. For purposes of comparison, the wear resistance of three metal materials (Ni-Hard cast iron, Raex 400 wear-resistant steel and structural steel S355) was included.

Based on the tests performed, it was observed that both epoxy-ceramic coatings Belzona 1811, ARC MX1 and ARC BX2, as well and polyurethane-based Belzona 2121 coating performed well in Taber wear test, when the type of wear was purely sliding abrasion without any impacts. On the other hand, epoxy-ceramic coatings did not perform well under slurry erosion while polyurethane-based coating did. The pull-off test results showed that epoxy-ceramic coatings greatly outperformed polyurethane-based coating and that conditioning the surface with a primer layer in ARC MX1 clearly improved adhesion. The application of these coatings to the substrate was relatively easy and did not require any special skill or equipment.

Key words
adhesion, abrasion, ceramic, coating, epoxy, erosion, polymer composite, polyurethane, pump, wear, wear resistance

CONCEPT DEFINITIONS

ASTM	American Society for Testing and Materials
at%	Atom percent
HBW	H from hardness, B from Brinell and W from the material of the indenter, tungsten (wolfram) carbide; unit of Brinell hardness test
HRC	Hardness Rockwell C, scale of Rockwell hardness test
HV	Vickers Pyramid Number, unit of Vickers hardness test
PA	Polyamide
PU	Polyurethane
SEM-EDS	Scanning Electron Microscopy - Energy Dispersive X-Ray Spectroscopy
UHMWPE	Ultra-high-molecular-weight polyethylene
vol%	Volume percent
wt%	Weight percent

ABSTRACT
CONCEPT DEFINITIONS
CONTENTS

GRAPHS

FIGURES

TABLES

1 INTRODUCTION

Industrial machinery and equipment usually experience progressive loss of material from exposed surfaces due to the relative motion between the exposed surface and another contacting surface. This progressive damage is called wear and it causes dimensional changes in the components of machines and equipment that lead to a decrease in their efficiency and lifespan. It is reported that about 23% of the annual global energy consumption, i.e., 119 EJ, is related to tribological contacts. Of this energy, 20% was destined to overcome friction and 3% corresponded to wear-related energy losses. (Holmberg & Erdemir 2017.) For that reason, understanding how wear works and how it can be prevented has become an issue of great importance and interest. Wear prevention can result in industries saving vast amounts of money by extending the lifespan of components and reducing downtime, maintenance costs and energy losses. It was estimated that 970 000 million euros could be saved over the next 15 years by implementing new technologies for friction reduction and wear protection (Holmberg et al. 2017).

Examples of wear are easy to find in any industrial facility (Nashett & Lyman 2015). For instance, industrial pumps are one of the pieces of equipment most susceptible to abrasive wear. They are required in a wide variety of industrial processes in diverse sectors, such as oil and gas, beverage, pulp and paper, pharmaceutical, and mining industries. Industrial pumps are designed to pump water and other products such as chemicals, petroleum, wastewater, oil, sludge, slurry or food, and are usually employed for heavy duty applications (All Pumps 2020). In these cases, pumps as well as pipes and other components that are part of the fluid handling equipment work in harsh environmental conditions and are subject to wear, corrosion, cavitation or a combination of these three phenomena (Smith & Kraenzler 2017). These processes cause damage to the pump which reduces its efficiency and can even lead to its failure.

The replacement or unscheduled repair of pump components, an entire pump or any other heavy-duty metal component can be costly. A more cost-effective alternative is the scheduled maintenance and preventive maintenance of components. This option involves the restoration of the components to the original dimension when necessary and the addition of a new layer of protection, which reduces the impact of wear on the components and reduces downtime and revenue loss.

Metallic coatings have traditionally been used for repairs, as they extend components lifespan and improve their performance. The most common repairing method used in the past was welding repair because it produced the most durable coatings. This method consists of cleaning the damaged areas, filling the space with an alloy to restore the original dimension if necessary, and welding the top with a material harder than the base material, e.g., stainless steel. However, the weld overlay repair technique requires high skill level and the material and labor repair costs are high. (Ruzga, Willis & Kumar 1993.)

Polymer coatings arose as a more affordable repair option and have been widely used on metal components to improve their tribological and mechanical properties. In this thesis two types of polymer coatings are studied: epoxy reinforced with ceramic particles and unreinforced polyurethane-based coatings. The study focuses on epoxy-ceramic reinforced coatings, which emerged on the market in the mid-90s. Over the years, these coatings have been reinforced with a wide range of ceramic particle types, sizes and volume fractions in matrix (Durand, Vardavoulias & Jeandin 1995). Polymer coatings have several advantages when compared to welding techniques, e.g., polymer coatings do not leave residual stresses that weaken the structure in the repaired components, labor costs are significantly lower, and better control of component contours through the use of templates is achieved (Ruzga et al. 1993).

Despite the popularity of wear-resistant polymer coatings, there are still many unanswered questions regarding fundamental understanding and engineering design issues, thus further research is necessary (Friedrich 2018). Several studies are published about the properties and wear resistance of polymer matrix ceramic reinforced composite coatings. However, few studies focus on coatings that contain large-size particles, i.e., larger than 1 mm. The size of the ceramic fillers depends directly on the size of the abrasive particles, thus these coatings should be used in the harshest wear environments, where the abrasive media consist of large particles.

The aim of this thesis was to study the applicability of polymer-ceramic composite coatings to replace metallic coatings in repairing of metal components. This thesis contains a brief literature review on polymer matrix reinforced with large ceramic particles composites, emphasizing on wear resistance and adhesion tests. In addition, the present study includes wear resistance and adhesion strength tests of different types of commercial epoxy-ceramic composite coatings. An unreinforced polyurethane (PU) coating was also tested. The test results are discussed, comparing the polymer coatings to each other as well as to reference metal materials.

The original idea of this study was to find a method to repair a worn pump impeller made of high chromium cast iron (popularly known in the industry as Ni-Hard), which is no weldable (FIGURE 1). This pump was operating at a pulp mill where it pumped woodchip-water slurry. Due to the erosion caused by the pumped fluid, the impeller experienced metal loss. To avoid further wear, which can lead to severe loss of efficiency or even to the pump failure, the possibility of rebuilding and re-profiling the eroded impeller with epoxy-ceramic cold-applied materials was considered.

FIGURE 1. Ni-Hard pump for which the coatings were originally designed. Left: impeller. Right: volute.

The present study is part of the project “CINEMA - Towards circular economy via ecodesign and sustainable remanufacturing”, which is funded by Interreg Nord. Centria University of Applied Sciences is one of the project partners along with Tampere University and Lulea University of Technology. The aim of the project is to strengthen the region’s competitiveness and economic growth as well as increase cross-border trade, export and internationalization of existing SMEs in the Interreg Nord region, with the help of the new business opportunities that a circular economy provides (Centria UAS 2020). Interreg Nord regions include north Norway, north Finland, north Sweden and Sápmi.

2 WEAR-RESISTANT COATINGS

2.1 Principles of wear: Wear mechanisms

According to ASTM International, wear is defined as the "damage to a solid surface, generally involving progressive loss of material, due to relative motion between that surface and a contacting substance or substances" (ASTM G40-02 2002). Wear is not an intrinsic material property but rather a complex process that depends on the whole tribological system or tribosystem. This system usually consists of two contacting bodies (i.e., a solid body and a counterbody), an interfacial element and an environment (FIGURE 2). The counterbody may be a solid, a liquid, a gas or a mixture of these. (Zum Gahr 1987, 82-83.)

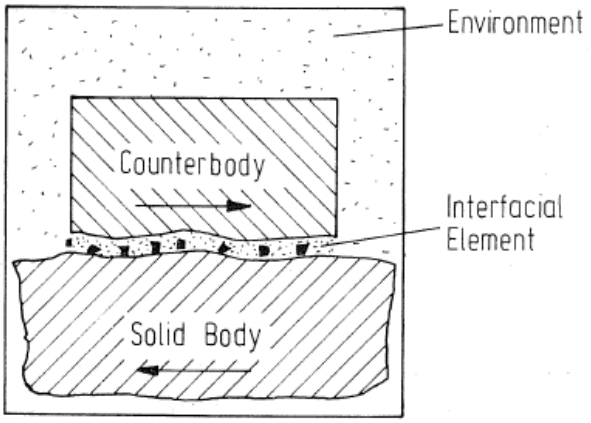

FIGURE 2. Schematic illustration of a tribological system or tribosystem (Zum Gahr 1987, 82)

Different wear modes may occur, and several classification criteria have been proposed and used in the literature. For example, wear modes can be classified according to contact type into sliding, rolling, impact, fretting, and slurry wear (Kato & Adachi 2000). Wear modes are also commonly classified based on the wear mechanism, as in the classification made by Budinski shown in figure 3. Budinski classifies wear modes by wear mechanism into abrasion, erosion, adhesive wear and surface fatigue wear (Budinski 2007, 24). These four wear mechanisms are described in the following sections.

Wear mechanisms are controlled by the parameters of the tribological system (Zum Gahr 1987, 80). Different wear mechanisms often occur at the same time, so it is important to understand each mechanism individually. Identifying the wear mechanisms that occur in an application is crucial to design or select wear-resistant materials that repair or prevent the wear damage. The tests carried out in this study focus on wear mechanisms that are most likely to occur on wear-resistant polymer coatings, i.e., abrasion and erosion.

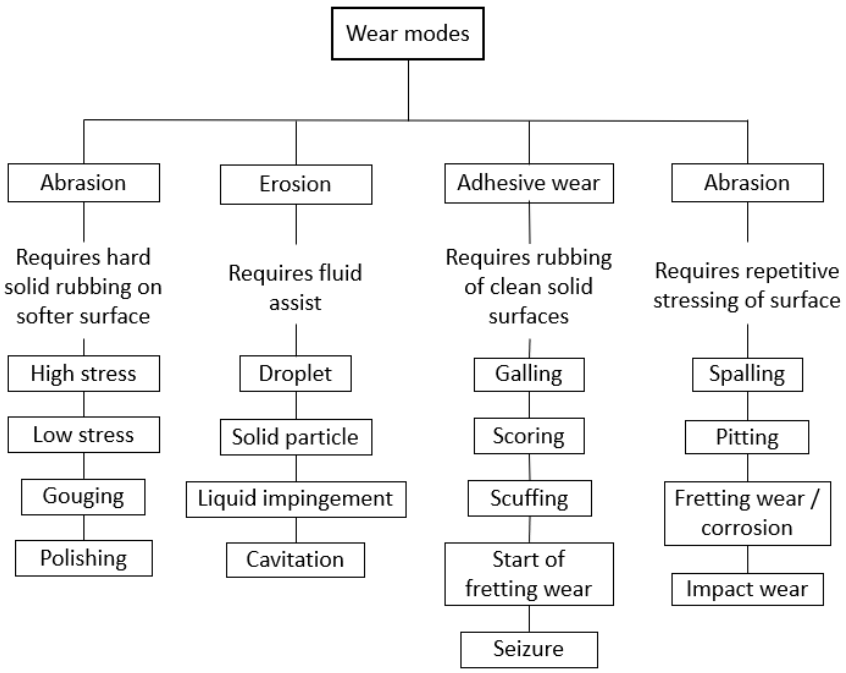

FIGURE 3. Wear modes classification based on wear mechanisms (adapted from Budinski 2007, 24)

2.1.1 Abrasive wear

According to ASTM G40-02 standard, abrasive wear is "wear due to hard particles or hard protuberances forced against and moving along a solid surface" (ASTM G40-02 2002). Different abrasion wear modes are: high stress, low stress, gouging and polishing (Budinski 2007, 24). The main abrasive wear mechanisms are micro-ploughing, micro-cutting, micro-fatigue, and micro-cracking (FIGURE 4) (Zum Gahr 1987, 96). Several of these mechanisms usually occur at the same time and they are controlled by different factors, e.g., surface hardness, particle size and hardness, and particle concentration.

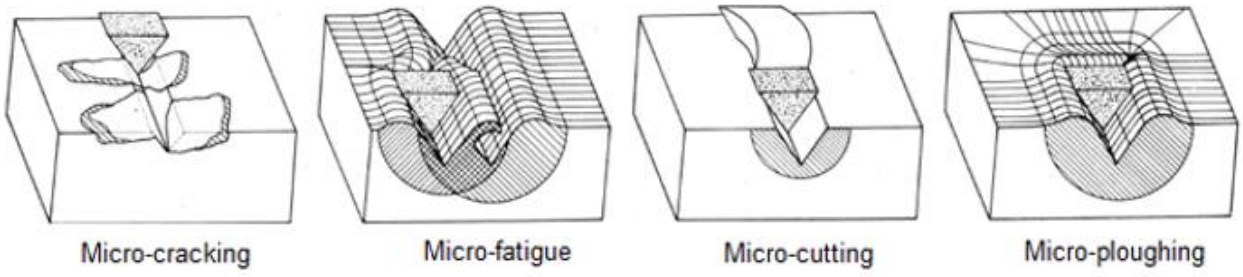

FIGURE 4. Schematic illustration of abrasive wear mechanisms (Zum Gahr 1987, 96)

Abrasive wear is commonly classified into two-body and three-body abrasive wear. In two-body abrasive wear, the hard particles or protuberances that cause wear on the solid body are fixed to the surface of the counterbody (FIGURE 5a) (ASTM G40-02 2002). In three-body abrasive wear, the hard particles are free to roll and slide between the solid body and the counterbody, acting as an interfacial element (FIGURE 5b). The wear in three-body abrasion is about one to two orders of magnitude smaller than in two-body abrasion. (Zum Gahr 1987, 95.)

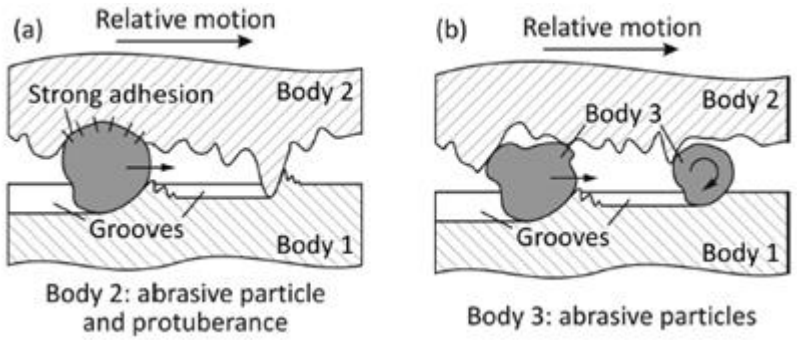

FIGURE 5. Schematic illustration of (a) two-body abrasive wear, and (b) three-body abrasive wear (Kandeva, Vencl, & Karastoyanov 2016)

2.1.2 Erosive wear

According to ASTM International, erosion is the “progressive loss of the original material from a solid surface due to the mechanical interaction between the surface and a fluid, a multicomponent liquid, or impinging liquid or solid particles” (ASTM G40-02 2002). Erosion includes several wear modes such as solid particle erosion, droplet erosion, liquid impingement erosion and cavitation erosion (Budinski 2007, 24). Another common erosion mode is slurry erosion, which is produced by a suspension of a

solid material in a liquid that impacts the surface of the solid body. The resistance of the wear-resistant coatings against slurry erosion was tested in this study.

Erosive wear involves several wear mechanisms including cutting erosion mechanism, fatigue erosion mechanism, plastic deformation, and erosion by brittle fracture (FIGURE 6). Wear mechanisms are controlled by many parameters such as particle physical properties (size, shape, and hardness), impingement angle, and impact velocity. (Agarwal, Chaudhary & Verma 2016.)

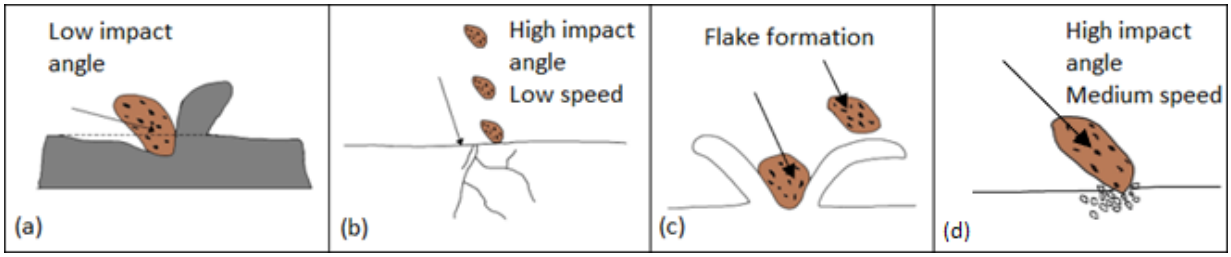

FIGURE 6. Schematic illustration of erosive wear mechanisms: (a) cutting erosion, (b) fatigue erosion, (c) plastic deformation, (d) erosion by brittle fracture (adapted from Agarwal et al. 2016)

A material can show either ductile or a brittle erosive behavior (FIGURE 7). In materials exhibiting ductile behavior, the exposed surface suffers from considerable plastic deformation around the points of impact, together with material removal. On the other hand, when materials exhibit brittle behavior, the exposed surface suffers little or no plastic deformation, but formation of cracks occurs. These cracks propagate, leading to a loss of material. For brittle erosion behavior the maximum erosion rate occurs at an angle near 90°, while for ductile erosion behavior it occurs at approximately 20-30º. (ASTM G40-02 2002.)

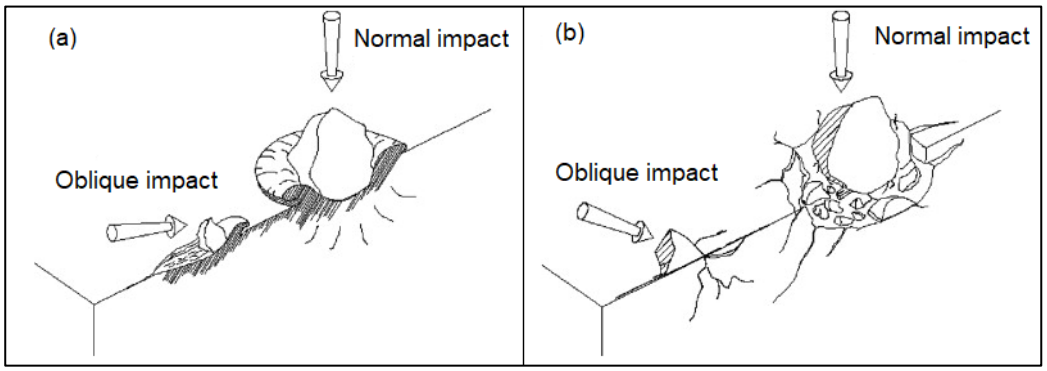

FIGURE 7. Schematic illustration of (a) erosive ductile behavior and (b) erosive brittle behavior (Wang & Yang 2008)

2.1.3 Adhesive wear

ASTM G40-02 standard defines adhesive wear as “wear due to localized bonding between contacting solid surface leading to material transfer between the two surfaces or loss from either surface” (ASTM G40-02 2002). Adhesive wear is characterized for high wear rates. Wear rate depends on the applied load, the sliding distance, the hardness of the softer surface, and the similarity of mating surfaces among other factors (Abdelbary 2014, 8). Adhesive wear occurs when two contacting surfaces experience a high pressure between the contacting asperities, which suffer large plastic deformation and bond to each other forming junctions (FIGURE 8). As one surface slides over another, junctions break due to shear stresses. As the sliding continues, wear debris might stay adhered to the opposing surface, adhere back to the original surface or become abrasive particles.

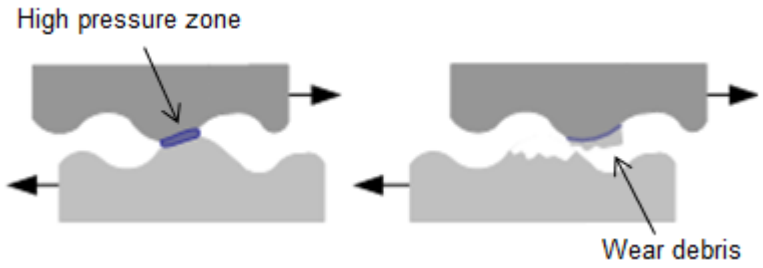

FIGURE 8. Schematic illustration of adhesive wear (Kopeliovich 2020)

Adhesive wear may occur with different grades of severity, i.e., mild, moderate and severe adhesive wear. Severe adhesive wear, also known as galling, occurs at a microscopic scale, and thus can lead to a catastrophic failure. Other forms of adhesive wear besides galling are scoring, scuffing, start of fretting wear and seizure (Budinski 2007, 24).

2.1.4 Surface fatigue wear

ASTM G40-02 standard defines fatigue wear as “wear of a solid surface caused by fracture arising from material fatigue” (ASTM G40-02 2002). Fatigue wear is characterized by crack formation and flaking of material caused by cyclic loading of solid surfaces, as shown in figure 9. Cyclic loading may originate from sliding and/or rolling contact of solids or impacting contact of solids and/or liquids. Some factors influencing fatigue wear rate are the frequency of cyclic stress, the contact pressure, and the surface properties. (Zum Gahr 1987, 99.)

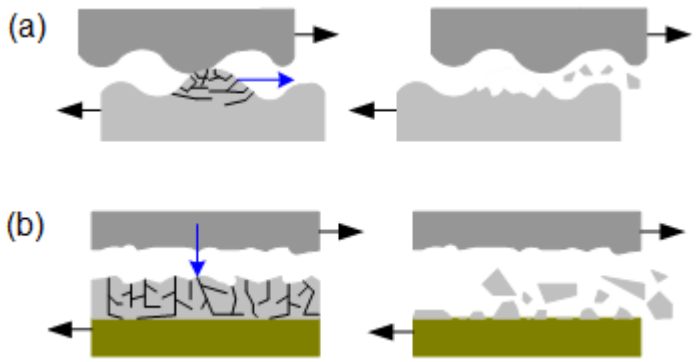

FIGURE 9. Schematic illustration of surface fatigue wear: (a) tangential cycling loading and (b) normal cycling loading (Kopeliovich 2020)

The fatigue of materials starts with elastic and plastic deformation, which is followed by work hardening and/or work softening. This leads to crack initiation with subsequent crack propagation until the final failure occurs (Zum Gahr 1987, 99). Cracks are formed either in the surface or in the subsurface of the material. The propagation of these cracks leads to material removal. Common modes of surface fatigue wear are spalling, pitting, fretting wear/corrosion, and impact wear (Budinski 2007, 24).

2.2 Wear-resistant coatings

A variety of coatings are designed to provide an extra layer of protection to surfaces of industrial equipment and machinery components. Applications of these protective coatings are found in every industry. The selection of coating depends on the component application. The application determines the environmental conditions in which the coating will work and, therefore, the requirements that it must meet. For example, in some applications coatings will be subjected to high levels of corrosion, e.g., in chemical industry, thus coatings with anti-corrosive properties will be required. In other applications coatings will be subjected to high levels of wear, e.g., in mining industry, thus wear-resistant coatings will be required.

Wear-resistant coatings consist of layers of usually hard materials carefully applied to the surface of components with the purpose of repairing worn-out components and/or protecting components against wear (Stachowiak & Batchelor 1993, 426). According to Davis (2001), there are different types of wear-resistant coatings depending on the coating deposition technique, including:

- organic coatings (i.e., paints and polymeric or elastomeric coating and linings),
- slip/sinter ceramic coatings, electroplating coatings (e.g., hard chromium coatings),
- electroless plating coatings (e.g., nickel-phosphorous and nickel-boron),
- weld overlays coatings (e.g., hardfacing alloys),
- thermal spraying coatings (e.g., many coating systems including ceramics and cermets),
- laser cladding coatings,
- carbide (salt bath) diffusion coatings,
- chemical vapor deposition coatings, and
- physical vapor deposition coatings (Davis 2001, 2).

Based on the material, coatings can be classified into metal coatings, ceramic coatings, polymer coatings, and composite coatings. Regarding metal coatings, some common materials include cadmium, chromium, copper, nickel, zinc and aluminum. Stainless steels, nickel alloys and other metal alloys are frequently used for coatings. Metal coatings can be deposited using some of the techniques commented previously (i.e., electroplating, electroless plating, thermal spraying, etc.). The properties of these coatings depend on the material and the application method but in general these hard coatings offer high corrosion and wear resistance. (A&A Coatings 2016.)

There are several types of protective ceramic systems. One of them consists of ceramic tiles or ceramic lining cylinders bonded to the surface of metal parts that need to be protected. Another type is ceramic coatings produced by plasma spraying, using ceramics such as alumina, titania, zirconia, chromia or a combination of them. These coatings offer high wear resistance, corrosion resistance, high hardness, and thermostability. (Precision Coatings Inc.)

Polymer coatings can include a wide range of materials such as urethane, epoxy, acrylic, nitrocellulose, silicone, natural or synthetic rubber, polyvinyl chloride, and phenolic resins (Inamuddin, Boddula, Ahamed & Asiri 2020). Different polymers offer different properties, but in general polymers are corrosion resistant, high-strength, lightweight and cost-effective materials (Sokol 2019).

A composite material is a combination of different materials that is designed to have a unique and superior combination of properties. Composite coatings include metal matrix composite (MMC), ceramic matrix composite (CMC), and polymer matrix composite (PMC) coatings. MMCs consist of a metal matrix reinforced with another metal or other material. For instance, a special type of MMC coatings is

metal-ceramic composite (i.e., cermet) coatings, which consist of a bend of ceramic and metallic powders processed using a variety of techniques. The most widely used cermet coating is thermally sprayed tungsten carbide/cobalt (WC-Co). Other common cermets are tungsten carbide/nickel-chrome (WC-NiCr), chromium carbide/nickel-chrome (Cr_3C_2- NiCr), and tungsten carbide/cobalt/chromium (WC-Co-Cr). (Improve Engineering System.) Cermet coatings are usually characterized by high temperature resistance, high hardness, high strength, chemical stability, and certain degree of plasticity (Yan, Deng, Su, Jiang, Chen, Cao & Liu 2019).

CMCs consist of a ceramic matrix reinforced with ceramic fibers. The purpose of the embedded particles is to improve the toughness of the monolithic ceramic matrix. Commonly used ceramic materials for both the matrix and the fibers are silicon carbide (SiC), alumina (Al_2O_3), carbon (C), and mullite or alumina silica (Al_2O_3-SiO_2) (L&L Special Furnace 2018). The desirable characteristics of CMCs include high-temperature stability, high thermal shock resistance, high hardness, high corrosion resistance, and light weight among others (Park & Seo 2011).

This study focuses on polymer composite coatings. Polymer composites consist of fibers (e.g., glass, carbon, and aramid) or fillers (e.g., ceramic beads or powder) embedded in a polymer matrix, which can be either a thermoplastic or a thermosetting polymer (Wu & Cheng 2006). The addition of reinforcement enhances the tribological behavior of polymers. Polymer-based coatings have become popular in a wide range of tribological applications owing to their self-lubrication ability, acceptable wear resistance, corrosion resistance, low frictional behavior, and durability. (Friedrich 2018.)

2.3 Wear-resistant ceramic-reinforced epoxy matrix composite coatings

Epoxy resin is a thermosetting polymer commonly used as a protective coating owing to its corrosion resistance, high strength, chemical stability, and strong bond ability. However, epoxy resins can be brittle and sensitive to micro-cracks. In order to improve their wear resistance and other properties such as adhesion, hardness, and corrosion resistance, epoxies can be filled with micro- or nanoparticles of ceramic oxides (e.g., Si_3N_4, ZnO, TiO_2, Al_2O_3, SiC, and SiO_2). The properties of the reinforced polymer are affected by the size, shape, dispersion uniformity and volume fraction in the matrix of the fillers. (Oliveira, Rocha & Galdino 2019.)

It has been proven that the wear resistance of epoxy can be significantly improved by adding a small content of nanoparticles. In the best cases, the wear rate decreased by three orders of magnitude. However, a quite large number of microparticles is usually required to achieve an evident enhancement of the wear resistance. (Mai & Yu 2006.) The strong interfacial bonding between the nanoparticles and the matrix due to high specific surface area of nanoparticles results in better tribological performance compared to that of the microcomposite (Devaprakasam, Hatton, Möbus & Inkson 2008). Although through the incorporation of fillers some of the changes are beneficial, some of them are adverse. Therefore, further efforts to understand wear mechanisms and improve the tribological performance are needed. (Mai et al. 2006.)

As mentioned in the introduction section, the size of the ceramic fillers used in the wear-resistant coating directly depends on the size of the abrasive media that will ultimately damage metal components. The epoxy-ceramic coatings investigated in this study were reinforced with large ceramic particles of alumina and silicon carbide, since they are designed to be used in highly abrasive environments (see Chapter 4.1 for more details of the studied coatings). Some of the advantages of these coatings include:

- coating is a solvent-free, cold-applied and cold-curing material
- coating application is easy (even on the curved surfaces) and any special equipment is needed
- it does not leave residual stresses to the substrate
- practically all metals can be coated (even the most unweldable ones)
- it can withstand practically all chemicals and does not corrode (Näkki 2019)

On the other hand, epoxy-ceramic coatings also have some disadvantages:

- the adhesion of the coating to the substrate is of concern
- it does not withstand high or low temperatures
- wear resistance cannot be at the same level compared with that of metal (matrix) materials with higher toughness (Näkki 2019)

Epoxy-ceramic composite coatings are an established technology for protection of components in different industries. The application range of these epoxy-ceramic coatings is immense. For instance, they are often used to provide wear and corrosion protection to industrial pumps. The application of these coatings on pumps increases pump efficiency, extends pump lifespan, eliminates additional costs, reduces downtime, and reduces wear impact among others (Belzona 2019).

In figure 10 it is shown how a polymer composite works on a worn substrate. As the substrate begins to suffer metal loss, the increasing turbulences accelerates wear. The polymer composite is applied to fill the pits caused by wear and is contoured to the required shape leaving it smooth with no ridges. Once the polymer composite is fully cured, it acts as a barrier between wear and the substrate.

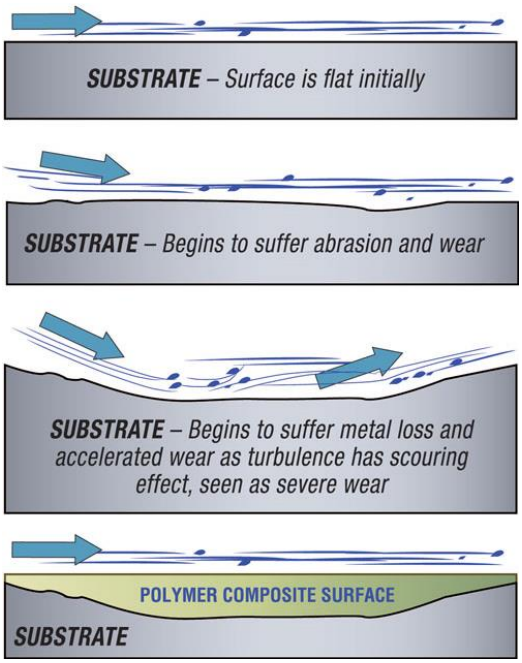

FIGURE 10. Polymer composite on a worn substrate (Nashett et al. 2015)

3 LITERATURE REVIEW

Polymer coatings are commonly reinforced with fillers, which can be particles or fibers, in order to improve their tribological and mechanical properties (Wu et al. 2006). There are several studies and publications about wear resistance and other properties of fiber-reinforced and particle-reinforced composites. However, it seems that these studies focus on different wear types or different environments, investigating composites reinforced with small hard particles (nanoparticles). This review will focus on those papers that investigate larger reinforcement particles (microparticles). The studies found in the following articles focus on those parameters that strongly influence the tribological performance of particle reinforced polymer composites, e.g., filler type, filler content, treatment to enhance the adhesion between fillers and matrix, and testing conditions.

It has been widely demonstrated that the addition of reinforcement particles to neat epoxy can improve its sliding wear resistance. For example, Oliveira et al. (2019) studied epoxy resins reinforced with micro Al_2O_3 particles and it was proven that the addition of these particles increased the adhesion, wear, and corrosion resistances of the epoxy resin. Al_2O_3 particles ranged from 5 to 15 μm and the volume fraction was 26%. Wear rates were calculated by using a Calowear abrasion tester and adhesion to the substrate was measured by using pull-off tests. The results showed that wear resistance of ceramic-loaded epoxy increased by 30% (i.e., wear rate decreased from $4{,}2 \times 10^{-11}$ m^2 N^{-1} to $2{,}9 \times 10^{-11}$ m^2 N^{-1}) and the adhesion to the substrate by 50% (i.e., adhesion strength increased from 20,4 MPa to 30,2 MPa). In addition, the effect of coating thickness on wear resistance was evaluated for thicknesses of 120 μm, 240 μm and 360 μm; and it was determined that increase of the thickness enhanced the resistance.

Fiber-reinforced epoxy-based composite also performed better than neat epoxy in the study carried out by Wu et al. (2006) They investigated the tribological properties of Kevlar pulp reinforced epoxy composites in both dry sliding and water lubricated conditions. Block-on-ring type friction and wear tester was used, with a sliding velocity of 0,42 m s^{-1} and a load of 100 N. Different volume fractions of 20, 40, and 60% were selected. It was found that the specific wear rate decreased with the volume fraction, obtaining the lowest wear rate value for a volume fraction of 40 vol%. Both pure epoxy and reinforced epoxy performed better under water lubricated than under dry sliding conditions. (Wu et al. 2006.)

However, in some studies it was demonstrated that unfilled epoxy performed better than filled epoxy. The interface between matrix and fillers is of high importance. If the interfacial bond is weak, the stresses

will not be correctly transmitted from the matrix to the fillers and the fillers will detach from the matrix, causing enhanced wear. Symonds and Mellor (1999) studied two epoxy-based coatings, one of them was ductile unfilled and the other one was filled with silica particles of different shapes and an average size of approximately 10 μm. Pin-on-wire wear test, pin-on-disc adhesive wear test and pin-on-disc abrasive wear test were carried out. The first test, which is a modification of the pin-on-disc test to measure wireline wear, was carried out applying loads from 0,3 to 6 N mm^{-1} at a sliding speed of 2,2 m s^{-1}. It was found that the reinforced epoxy had a higher wireline wear resistance than the ductile coating, under a load not greater than 3 N mm^{-1}. However, in the abrasive test, where a load of 10 N and speeds of 0,26 and 2,6 m s^{-1} were applied, ductile epoxy performed better than the filled epoxy coating especially at low sliding speeds. In the adhesive wear test, where loads of 20, 40, 80 and 160 N and speeds of 0,26, 0,52, 1 and 2,6 m s^{-1} were applied, the wear rates of both coatings were very similar and low. (Symonds & Mellor 1999.)

Regarding the reinforcement particle size, studies generally show that better wear resistance is obtained with smaller reinforcement particles. For instance, in the study by Palraj, Meena, Maruthan and Rajagopal (2015) it was demonstrated that nano silica epoxy composite coating offered better wear resistance than micro silica coating. In the study by Chang and Hazizan (2013) the weight loss due to wear for nano-ZnO/UHMWPE composites was lower compared to that of micro-ZnO/UHMWPE and pure UHMWPE.

Ahmedizat, Al-Zubaidi, Al-Tabbakh, Achour and Hamead (2019) used nano- and microparticles of Al_2O_3 to reinforce glass fiber/epoxy composite. Glass fiber volume fraction was 3%, while the weight fractions of Al_2O_3 particles were 2%, 4% and 6%. The average diameter of Al_2O_3 nano-powder was 45 nm and for Al_2O_3 micro-powder it was 1,914 μm. The wear resistance tests were carried out on a home-made wear tester, applying different impact angles and different abrasive particle sizes. Based on the results, glass fiber/epoxy composite outperformed neat epoxy resin. In addition, composite filled with nanoparticles presented higher erosion resistance than composite filled with microparticles, which showed lower erosion rates than glass fiber/epoxy composite and pure epoxy. (Ahmedizat et al. 2019.)

Wetzel, Haupert, Friedrich, Zhang and Rong (2001) also used nano- and microparticles to reinforce neat epoxy. They used SiC microparticles with an average particle diameter of 10 μm and 5 μm and TiO_2 nanoparticles with an average size ranging from 200 to 400 nm. A block-on-ring wear test was used, applying a pressure of 1 MPa and a sliding speed of 1 m s^{-1}. The specific wear rate of TiO_2 nanocomposite was reduced by 92% from that of neat epoxy at a filler content of 7,5 vol%. The specific wear rate

of 10 μm SiC and 5 μm SiC reinforced composites was reduced by 54% and 73%, respectively, at a filler content of 17,5 vol%. The results revealed that the stiffness and specific wear rate of the microcomposite improve, whereas the impact toughness suffered. The nanocomposites demonstrated an improvement of stiffness, toughness and wear. (Wetzel et al. 2001.)

However, some studies reported that bigger particle size leaded to better tribological performance. For example, in the study carried out by Durand et al. (1995) the dry sliding wear behavior of polymer-based composites reinforced with ceramic particles was investigated. Several experiments were performed using different ceramic particle types, i.e., Al_2O_3, TiC, SiC, TiN, VC, TiO_2, and ZrO_2, different mean particle sizes from 5 to 100 μm and different particle volume fractions from 5 to 40%. A pin-on-disc tester was used for measuring the wear rate, applying a normal load of 10 N and a sliding velocity of 0,1 m s^{-1}. For the given test conditions, the results showed that the wear rate decreased up to 50 times for composites containing 20 vol% of ceramic particles (8×10^{-15} m^2 N^{-1}), whereas increasing this volume fraction did not significantly improve the wear resistance. In addition, it was found that for the particle size larger than 20 μm carbide particles performed better than oxide particles, and large particles of about 100 μm protected better than small particles of about 20 μm, which did not protect since they were removed along with the polymer debris. (Durand et al. 1995.)

Another example is the study by Cinar, Ozmen Eruslu, Savas Dalmis and Guven (2019). They investigated the effect of the size and shape of the fillers on the wear resistance of reinforced epoxy coatings. The different shapes of the glass particles used were spherical, flake, rod, and irregular shape. A pin-on-disc tribometer was used for testing the dry-sliding wear and the weight loss was measured. It was concluded that the most effective shapes for reducing the weight loss, i.e., for increasing the wear resistance, were irregular-shaped particles (> 50 μm) and spherical-shaped particles. On the other hand, flake and fiber particle had an adverse effect on wear resistance, while epoxy reinforced with irregular-shaped particle (< 50 μm) performed similar to neat epoxy. Wear resistance as well as wear mechanisms were affected by the size and shape of the reinforcement particles and also by their aspect ratio; the higher the aspect ratio, the lower the wear resistance. (Cinar et al. 2019.)

A higher wear resistance for larger reinforcement particles was also obtained in the study carried out by Schramm, Dwars and Kühl (2005). Several commercially available coating materials with both epoxy and polyurethane based matrix were investigated. A blast wear test stand was used for evaluating the resistance to wear, spraying a mixture of sharp sand and water onto the specimens at a velocity of 15 m

s-1 with an impinging angle of 45°. Among the total of 27 tested coatings, only thick trowelling compounds containing large SiC and/or Al_2O_3 particles as well as unreinforced polyurethane coating materials showed wear rates comparable to those of grey cast iron while no coating showed wear rates comparable to those of white iron. A cavitation test was also performed and all coatings failed quickly; the best results were obtained by unreinforced polyurethane-based coatings. (Schramm et al. 2005.)

As commented previously, the adhesion between the filler and the matrix is of great importance and it can be further increased with a chemical reaction between them. The chemicals used to promote adhesion between an organic and an inorganic substrate are called coupling agents (Pape 2011, 503). Jia and Ling (2005) investigated the influence of Al_2O_3 particles treated with a silane coupling agent on the abrasive wear resistance of Al_2O_3/PA1010 composite coatings. The test instrument used in this case was a turnplate abrasive wear testing machine JMM. The size of the Al_2O_3 particles ranged from 40,5 to 161,0 μm and the particle volume fraction ranged from 5 to 22%. In the study it was concluded that when the Al_2O_3 particles were treated with a coupling agent, the wear resistance notably improved. In addition, the wear resistance of Al_2O_3/PA1010 composite coatings increased linearly with the increase of the volume fraction of Al_2O_3 particles, with a linear correlation coefficient of 0,979. In this study it was found that the particle size did not seem to influence the abrasive wear resistance.

In the investigation presented by Fengkun, Yuqin, Shuqin, Dongbo, Shiyuan, Feng, Baozhang, Zhangzhong and Pingze (2019) epoxy resin was reinforced with unequal flakes and irregular particles of Al_2O_3 (46 wt%) ranged from 1 to 10 μm and spherical particles of WC-Co (29 wt%) ranged from 5 to 25 μm. The two coatings obtained were applied on top of TC18 titanium alloy (Ti-5Al-5Mo-5V-1Cr-1Fe) by air spraying process and reciprocating dry sliding wear was tested with sliding loads and velocities of 400 g - 400 r/min and 700 g - 500 r/min, respectively. It was found that the wear resistance of the epoxy/Al_2O_3 coating increased by 64,7%–69%, while the epoxy/WC-Co coating increased by 59,4%–62%, compared to TC18 titanium alloy substrate. In conclusion, epoxy/Al_2O_3 coating was superior to epoxy/WC-Co coating, and the substrate was the worst. In addition, the adhesion of the coatings was tested by cross-cutting test and both coatings had the same level of adhesion, i.e., “a little spalling, spalling area was less than 5%”. (Fengkun et al. 2019.)

Vijay, Soti, Banerjee and Sierros (2019) compared the abrasion resistance of vinyl-based coatings and different polymer composite coatings, including two polymer-ceramic composites (ARC 855 and ARC S2) composed of modified epoxy resin and silicon carbide flakes as a reinforcement. A Taber reciprocating abrader was used, and the results showed that reinforced polymer composite coatings performed

significantly better than the vinyl-based coatings. The wear rate obtained on vinyl coatings was 1,4–5,7 and 7–52 times higher than that of polymer–ceramic coatings under dry and wet conditions, respectively. In addition, ARC 855 performed better than ARC S2 under dry surface abrasion with a volume loss 3,6 times lower, while ARC S2 performed better under wet conditions, with a volume loss 5,5 times lower than that of ARC 855. (Vijay et al. 2019.)

Regarding solid particle erosion applications, it is not well-established that the addition of reinforcement particles to a polymer matrix can improve its erosion resistance. There are few studies about it and both increases and decreases in the erosion rate have been reported for an increased reinforcement volume fraction. (Arani, Rabba & Papini 2019.) Zhou, Lu, Jiang and Li (2005) investigated the erosion resistance and mechanical properties of polyurethane matrix composites reinforced with Al_2O_3 particles (0–64 wt%). The results showed that the tensile strength and the elongation at rupture decreased, the hardness increased gradually, and the erosion resistance first increased until reaching a maximum and then decreased, with the increasing content of Al_2O_3 particles. (Zhou et al. 2005.) Zahavi and Schmitt (1981) investigated the erosion resistance of polymers reinforced with quartz and glass particles. The results revealed that the reinforced composites had a lower erosion resistance compared to that of neat polymer, and it decreased by increasing the reinforcement volume fraction. (Zahavi et al. 1981.)

The erosion resistance of polymers reinforced with large particles had not been properly investigated until Arani et al. studied the solid particle erosion of epoxy matrix composites reinforced with Al_2O_3 spheres with an average diameter of 194 μm and 447 μm. Solid particle erosion tests were performed using an AccuFlo AF10 micro-abrasive blaster, at particle velocities of 121, 83, and 90 m s^{-1} for the 22 μm, 97 μm and 152 μm irregular shaped SiC abrasive particles, respectively. Reinforcement volume fractions of 25%, 35% and 45% were used. According to this study, three dimensionless ratios influence notably the erosion resistance: the abrasive to reinforcement particle size (r_1), the abrasive particle size to the average edge-to-edge distance between reinforcements (r_2), and the abrasive particle kinetic energy to a threshold kinetic energy (r_3). Arani et al. found that at perpendicular incidence, modest improvements in erosion resistance could be obtained at intermediate r_2 values ($1 < r_2 < 3$) when r_1 was intermediate ($0{,}2 < r_1 < 0{,}35$). At oblique incidence, the erosion resistance of the composites was significantly higher than the neat epoxy in all cases. It was also demonstrated that the composites erosion resistance improved with the use of a coupling agent. (Arani et al. 2019.)

The behavior of hybrid composites (i.e., composites reinforced with both fibers and particles) under solid particle erosion has been investigated in some papers, but it has not been extensively studied yet.

For example, Ahmedizat et al. (2019) compared the erosion rates of neat epoxy, glass fiber (GF) reinforced epoxy composite and GF/micro-Al_2O_3 reinforced epoxy composite. The maximum erosion rate reduction was about 92% from that of neat epoxy and it was achieved with the addition of 3 vol% glass fibers and 6 wt% of alumina particles (average size 1,914 μm), at an impingement angle of 60º. It was demonstrated that erosion resistance increased with increasing reinforcement weight fractions. (Ahmedizat et al. 2019.) Patnaik, Satapathy and Mahapatra (2007) investigated the solid particle erosion of a hybrid composite as well. A polyester matrix reinforced with glass fibers and Al_2O_3 particles with an average size of 50 μm was studied. Filler contents of 0 wt%, 10 wt% and 20 wt%, and impingement angles of 45º, 60º and 90º were used. It was concluded that the erosion resistance of hybrid composite was higher than that of fiber-reinforced composite. (Patnaik et al. 2007.)

World Pumps magazine contains several articles of case studies in which epoxy-based composite coatings were applied on pumps obtaining great results; extending the pumps lifespan and avoiding downtime and replacement costs. However, these articles are published by the manufacturer company of these coatings (i.e., Belzona) so the information should be considered biased. For example, in 1999 the pumps from a fish farm were internally coated with an epoxy-based coating material (Belzona 1341) to protect them from erosion and corrosion. The coating improved the efficiency of the pumps and saved the company operating costs, and additionally after 15 years the pumps were still in service. Belzona manufacturers sustain that applying this coating material increases of efficiency up to 7% on new equipment and up to 20% on refurbished equipment have been achieved. (Belzona 2014.)

In another case study, a Ni-Hard slurry pump from a nickel and cobalt refinery was repaired using different ceramic filled epoxy-based composite coatings for each component (i.e., Belzona 1311, Belzona 1321, and Belzona 1812). In addition, a layer of ceramic filled epoxy composite Belzona 1391 was applied on the internals and a corrosion resistant epoxy-based coating Belzona 5891 was applied on the externals. (Belzona 2015.) In a paper mill a cast iron submersible sludge pump was also coated with ceramic filled epoxy-based composites. Belzona 1311 was used for restoring the pump to the original dimension, and then Belzona 1321 was applied on the internal surfaces of the pump and Belzona 5811 on the external surfaces. After six year of service they claim that the coating is still in excellent condition. (Belzona 2017.) Another article tells about how in 1980 two heavily corroded cooling water pumps from a power station were repaired and protected with ceramic-filled epoxy-based composite coatings. They were coated both internally and externally and later over coated, the internals with Belzona 1321 and the externals with Belzona 1341, extending considerably the lifespan of the pumps. (Belzona 2018.)

In addition, on Belzona website there is a database with hundreds of examples of Belzona know-how in action. For example, ceramic reinforced epoxy-based composite Belzona 1811, one of the coatings studied in this thesis, has successfully been applied multiple times on different components in different industry sectors throughout the years. In a coal mill it was applied on eroded steel spinner blades to restore them to original dimension (Belzona, Know-how in action 11 No 21). The internal surface of a stainless steel gravel slurry pump used in mining was also coated with Belzona 1811 (Belzona, Know-how in action 28 No 126). In a paper mill it was applied on a steel rotating de-barker drum, since its steel protection plates were failing due to severe abrasion. (Belzona, Know-how in action 32 No 11). Severe abrasion was also the reason why inside surfaces of the steel pipe elbows in a copper and gold mine were coated. (Belzona, Know-how in action 23 No 76). In other case, steel pipes and valves used to transport cement dust in a cement plant were repaired with Belzona 1811 as well (Belzona, Know-how in action 26 No 34).

On the website of Chesterton company, there are also several publications of case studies using ARC MX1, which is one of the coatings studied in this thesis, and other products used on water pumps and slurry pumps. They show how the application of epoxy-ceramic coatings leads to reduced costs and downtime. For example, ARC MX1 was applied on a pump wear plate that showed severe abrasive wear from iron powder slurry (Chesterton, Case study 084). It was also effectively applied on seal adaptor plates from a limestone slurry pump that worked in harsh environmental conditions (Chesterton, Case study 128), and on a Tech-Taylor valve dealing with highly abrasive slurry (Chesterton, Case Study 115).

In some applications, ARC MX1 has been used together with other coating materials, such as ARC 855, to achieve better results. These two coatings were applied, for instance, on both the case and impeller of a split case slurry pump in order to improve its efficiency and protect it from abrasion and corrosion (Chesterton, Case Study 111). Also ARC MX1 and ARC BX2 are sometimes used together to repair and protect pumps and, as a matter of fact, the purpose of this study was to use both materials to repair the worn Ni-Hard pump housing shown in figure 1. These two epoxy composites were applied on flue gas desulfurization slurry pumps that suffered a loss of efficiency due to its severe corrosion/abrasion (Chesterton, Case Study 015). Both composites were also used to replace a rubber lining of a limestone slurry recirculation pump, since the rubber lining suffered delamination (Chesterton, Case Study 104).

A study by Verosky, Maier, White, Connell, Knoll, King, Hanley and Metzger (2008) was published in Pumps & Systems magazine. In the study they investigated the pump efficiency increase obtained by

mechanical refurbishment and coating. In a pilot study the internal surface of three pump cases was coated with epoxy-ceramic coatings. For the three pumps, the results showed that the pump efficiency increased by more than 8% from sandblasting and coating, and all three pumps were approximately returned to original manufacturer pump curves. (Verosky et al. 2008.) Based on these results, a new research on the use of these coatings to improve pump efficiency was conducted. In this study, 18 pumps were coated with brush-on epoxy-ceramic coatings. The results showed an average efficiency increase of about 12%; 5% from mechanical refurbishment, 6% from coating the internal pump casing, and about 1% from coating the impeller. The pumps that were coated had higher efficiencies and kept those efficiencies longer than those pumps that were only sandblasted. (Maier & King 2009.)

4 MATERIALS AND METHODS

This chapter presents the materials studied in the experimental part of this thesis, i.e., epoxy-ceramic coatings Belzona 1811, ARC MX1 and ARC BX2; polyurethane-based coating Belzona 2121; and metal materials Ni-Hard cast iron, Raex 400 steel and S355 steel. In this chapter, also the preparation of the test samples is explained in detail as well as the procedures followed to examine the samples (SEM/EDS analysis) and to test their adhesion strength, slurry-erosion resistance and sliding-abrasion resistance.

4.1 Epoxy-ceramic coatings

Three commercially available trowel-on epoxy-ceramic coating materials were chosen to be tested. They are two-component composites, consisting of an epoxy resin as the matrix and ceramic particles as the reinforcement. These materials are used to restore worn equipment to original dimensions and to protect the surfaces that are subjected to different levels of abrasion. The aforementioned coatings are: Belzona 1811, Chesterton ARC MX1 and Chesterton ARC BX2, products of Belzona Polymerics Limited Company and A.W. Chesterton Incorporated Company, respectively. As commented in 2.3, these coatings are safe to use since they are solvent-free, they are cold-applied and cold-curing materials, and they are easy to apply even on curved surfaces without special tools.

4.1.1 Belzona 1811

Belzona 1811 (Ceramic Carbide) is an epoxy-based composite that comes with two components, a base that contains hard angular particles, and a solidifier. These hard particles are relatively large since the coating is designed to protect metal surfaces against large abrasive particles.

According to the manufacturer, Belzona 1811 offers high abrasion resistance, high mechanical strength, long working life, and short curing time which minimizes downtime. The values of these material properties as well as other technical data can be seen in table 1. In addition, Belzona 1811 has excellent corrosion resistance and it bonds well to metal surfaces including steel and cast iron. (Belzona 2020.) Belzona 1811 can be used in numerous industries. It can be applied on a wide variety of components such as pipes, elbows, valves, wear plates, screw conveyors, pump impellers, hoppers, chutes, mixing

bowls, mixer blades and other equipment subject to abrasion (Belzona 2020; Belzona Product Flyer: Belzona 1811).

TABLE 1. Technical data of Belzona 1811 (adapted from Belzona Product Flyer: Belzona 1811; Belzona Product specification sheet: Belzona 1811)

Cured Density	0,00218 g/mm³
Working life	60 minutes at 20 °C
Time to full mechanical cure	3 days at 20 °C (thickness of about 6 mm)
Dry heat resistance	200 °C
Abrasion resistance - Taber with 1 kg load (ASTM D4060)	H10 Wheels (Wet) - 57 mm³ loss per 1000 cycles
	CS17 Wheels (Dry) - 7 mm³ loss per 1000 cycles
Adhesion - Tensile shear (ASTM D1002)	16,55 MPa on blasted mild steel
Flexural strength (ASTM D790)	37,23 MPa
Compressive strength (ASTM D695)	77,91 MPa
Minimum thickness	6 mm
Shelf life (unopened containers)	5 years (stored between 0 °C and 30 °C)

4.1.2 Chesterton ARC MX1

The matrix of Chesterton ARC MX1 composite is an epoxy resin reacted with an aliphatic amine curing agent and the reinforcement is a mixture of spherical alumina (Al_2O_3) and silicon carbide (SiC) particles pretreated with polymeric coupling agent. ARC MX1 differs from the other test materials since it comes with a total of 5 components. It has a separate primer coating material with two components, parts A (resin) and B (hardener) that do not contain hard particles. The purpose of this primer layer is apparently to ensure the good adhesion to the substrate. The actual coating material consist of three components, parts A (resin), B (hardener) and C (white spherical particles). The reinforcement alumina particles are relatively large as ARC MX1 is designed to protect metal surfaces against sliding wear and impact caused by medium to large particles.

Chesterton manufacturers assure that ARC MX1 coating offers extreme abrasion and impact resistance, resisting a wide range of slurries and resisting repeated high impact forces. Table 2 shows some of its technical data. ARC MX1 withstands chemical attack, it presents high adhesion strength and it cures at room temperature in a short time (TABLE 2). (Chesterton Product datasheet: ARC MX1.) ARC MX1

can be applied, for example, in pulverizes, hoppers and silos, conveyor screws, water and slurry pumps, slurry pipelines and pipe elbows, wear plates, blowers and cyclones, fan housings, ceramic tile lined chutes, and pneumatic pipelines (Chesterton Product datasheet: ARC MX1).

TABLE 2. ARC MX1 technical data (adapted from Chesterton Product datasheet: ARC MX1)

Cured Density	0,0026 g/mm^3
Working life	30 mins at 25 °C (ARC MXP Primer 20 mins at 25 °C)
Time to full mechanical cure	20 hours at 25 °C
Temperature resistance	Wet Service 95 °C
	Dry Service 205 °C
Compressive Strength (ASTM C 579)	73,7 MPa
Flexural Strength (ASTM C 580)	34,4 MPa
Pull off Adhesion (ASTM D 4541)	22,1 MPa
Tensile Strength (ASTM C 307)	25,9 MPa
Impact Resistance (Direct) (ASTM D 2794)	67,7 N-m
Shore D Durometer Hardness (ASTM D 2240)	89
Vertical Sag Resistance	No Sag at 21°C and 6 mm
Slurry Abrasion Response (SAR) (ASTM G 75)	1,78
Minimum thickness	6 mm
Shelf life (unopened containers)	2 years (stored between 10 °C and 32 °C)

4.1.3 Chesterton ARC BX2

The matrix of Chesterton ARC BX2 is a modified epoxy resin reacted with an aliphatic amine curing agent and the reinforcement is a blend of medium to fine sintered bauxite beads and fine SiC powders treated with polymeric coupling agent. ARC BX2 material comes with two components, a part A (resin) that contains spherical particles, and a part B (hardener).

This coating is designed to protect surfaces subjected to moderate sliding abrasion, i.e., fine abrasive particles. ARC BX2 offers some benefits such as high adhesive strength which provides it with disbonding resistance, short curing time which reduces downtime, and chemical resistance to a broad range of chemical attacks. Table 3 shows ARC BX2 technical data. (Chesterton Product datasheet: ARC BX2.) Some examples of applications of ARC BX2 industrial coating include slurry pumps, conveyor screws,

slurry pipelines, pipe elbows, pipe spools, hoppers and silos, hydropulpers, wear plates, chutes, fan blades and housings, hydro-cyclones, and turbo separators (Chesterton Product datasheet: ARC BX2).

TABLE 3. ARC BX2 technical data (adapted from Chesterton Product datasheet: ARC BX2)

Cured Density	0,0021 g/mm^3
Working life	25 - 35 minutes at 25 °C
Time to full mechanical cure	36 hours at 25 °C
Maximum Temperature	Wet Service 95 °C
	Dry Service 205 °C
Pull-Off Adhesion (ASTM D 4541)	> 21 MPa
Compressive Strength (ASTM C 579)	98 MPa
Flexural Strength (ASTM C 580)	54 MPa
Tensile Strength (ASTM C 307)	27 MPa
Impact Resistance (reverse) (ASTM D 2794)	18 N-m
Linear Coefficient of Thermal Expansion (ASTM C 531)	3,5 x 10-5 cm/cm/°C
Shore D Durometer Hardness (ASTM D 2240)	90
Vertical Sag Resistance	No sag at 21°C and 6 mm
Minimum thickness	3 mm
Shelf life (unopened containers)	2 years (stored between 10 °C and 32 °C)

4.2 Polyurethane-base coating

Belzona 2121 was the only unreinforced polyurethane-based coating tested in this study. Belzona 2121 is a product of Belzona Polymerics Limited Company and it comes with two components, a base and a solidifier. However, so ensure the adhesion to the substrate, the surface should be conditioned with Belzona 2911 or 2921 before applying Belzona 2121.

Belzona 2121 (D&A Hi-Coat Elastomer) is a flexible and tough rubber material designed to protect metal and rubber surfaces subjected to high levels of wear, impact and abrasion. According to the manufacturer, Belzona 2121 offers high mechanical strength, high elongation, excellent durability, and excellent chemical resistance to a broad range of chemical attacks. It demonstrates an outstanding adhesion to a wide range of substrates, e.g., rubber, PVC, aluminum, copper, steel, cast iron, lead, glass, wood, most plastics, and concrete. Some technical data of Belzona 2121 coating is shown in table 4. (Belzona Product Flyer: Belzona 2121.) Belzona 2121 is suitable for application on pump casings and impellers,

pipes, tanks and fluid handling equipment, ship propellers, and vibrator feed bowls among others (Belzona Product Flyer: Belzona 2121).

TABLE 4. Belzona 2121 technical data (adapted from Belzona Product Flyer: Belzona 2121)

Cured Density	0,00115 g/mm3
Working life	12 minutes at 20 °C
Time to full mechanical cure	24 hours at 20 °C
Temperature resistance	Wet Service 40 °C
	Dry Service 90 °C
Abrasion resistance - Taber with 1kg load (ASTM D4060)	H10 Wheels (Wet) - 27 mm³ loss per 1000 cycles
	CS17 Wheels (Dry) - 31 mm³ loss per 1000 cycles
Adhesion 90º peel (ASTM D429 modified)	3020 kg/m on mild steel
Elongation	500-600 % after 24 hour cure at 20 °C
Shore A Hardness (ASTM 2240)	89 after 24 hour cure at 20 °C
Minimum thickness	0,8 mm
Shelf life (unopened containers)	3 years (stored between 5 °C and 30 °C)

4.3 Reference materials

Epoxy-ceramic coatings can be used to replace metal as wear-resistant material. For purposes of comparison, the wear resistance of three metal materials (Ni-Hard cast iron, Raex 400 wear-resistant steel and structural steel S355) was tested. All these reference metal materials are described in this chapter.

4.3.1 High chromium cast iron material (Ni-Hard)

High chromium white cast iron is an extremely abrasion resistant and relatively hard cast iron (~550 HBW). It also offers reasonable corrosion resistance. Heat treatments, such as hardening, tempering and soft annealing, are commonly used to improve its properties (SFS-EN 12513 2011). High chromium cast iron is used in many different industries, e.g., mining, cement, and milling industries. The applications of this cast iron include slurry pumps, mill liners, cyclones, chute liners, pipes and elbows. (Penticton Foundry 2017.)

Different grades of Ni-Hard exist, depending on its composition. Ni-Hard cast iron samples were machined from a larger part that had been cut off from the pump impeller shown in figure 1. Its composition was measured with a Hitachi handheld X-ray fluorescence spectrometer (XRF). The results of the spectrometry are shown in table 5. The composition of the impeller fits that of high chromium cast iron 5.5610 according to the standard SFS-EN 12513. This grade contains the highest level of chromium of the chromium white iron alloys, i.e., 23-30%. (SFS-EN 12513 2011.) The hardness of the pump impeller material was measured from the cross-section, obtaining a value of 600-650 HV (~ 55 HRC). Microstructure of this Ni-Hard cast iron is shown in figure 11. The black areas indicate microporosity in a cast material.

TABLE 5. XRF analysis results for the impeller and chemical composition of cast iron 5.5610 according to SFS-EN 12513 (wt%) (SFS-EN 12513 2011)

	C	Si	Mn	Al	P	S	Ti	V	Cr	Fe	Ni	Mo	Cu
XRF	NA	0,7	1,4	0,1	0,03	0,1	0,1	0,1	**26,0**	69,8	0,9	0,0	0,9
5.5610	1,8 – 3,6	max 1,0	0,5 – 1,5	–	max 0,08	max 0,08	–	–	**23,0 – 30,0**	the rest	max 2,0	max 3,0	max 1,2

**NA – Not available*

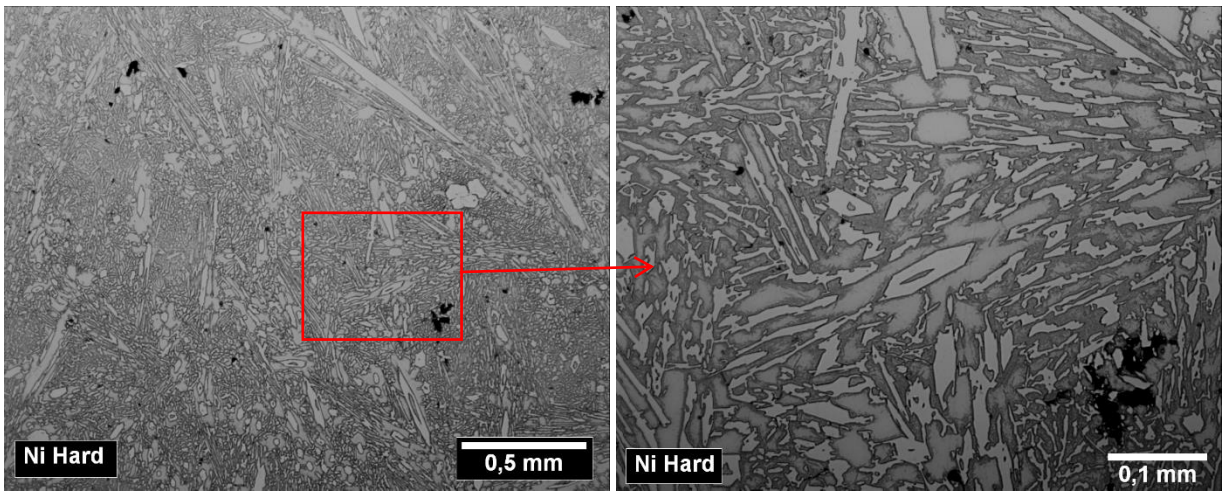

FIGURE 11. Optical microscope image of microstructure of Ni-Hard cast iron

4.3.2 Wear-resistant steel (Raex 400)

Raex 400 is a wear-resistant steel manufactured by SSAB in Finland, which presents an average hardness of 400 HBW and a typical yield strength of 1100 MPa. It is a steel with favorable hardness, high impact toughness, good bending properties, high surface quality and flatness, and relatively good weldability. Raex 400 is ideal for many applications such as loading buckets and dump truck bodies, lining equipment parts, and conveyor systems in mining industry. Raex 400 is also used for equipment and machinery in concrete industry, agriculture industry and road construction industry. The chemical composition of a quenched and tempered Raex 400 sheet is shown in table 6 and its microstructure is shown in figure 12. (RAEX 2020.)

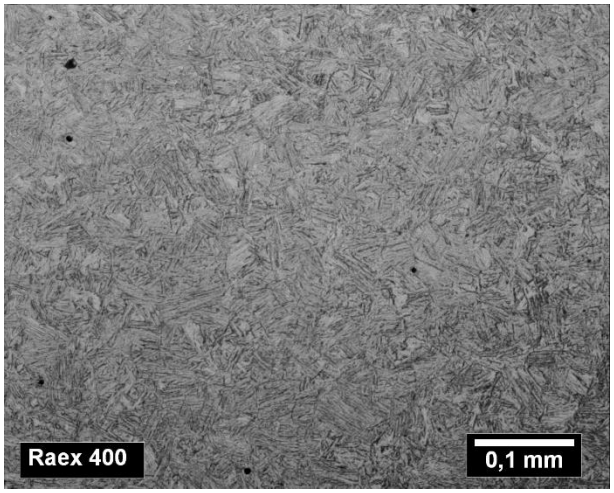

FIGURE 12. Optical microscope image of microstructure of Raex 400 wear-resistant steel

TABLE 6. Chemical composition of Raex 400 sheet plates (wt%) (Hardox 400 - datasheet)

C	Si	Mn	P	S	Cr	Ni	Mo	B	Typ CET (CEV)
max 0,16	max 0,50	max 1,60	max 0,025	max 0,010	max 1,20	max 1,00	max 0,25	max 0,005	0,30 (0,48)

4.3.3 Structural steel S355

S355 is a non-alloy structural steel with great welding and machining properties, and a maximum hardness of 146-187 HB. Structural steel grades are named based on the minimum yield strength of the steel tested at a thickness of 16 mm. Therefore, S355 steel with a thickness of 16 mm offers a minimum yield strength of 355 MPa. (Gilbert 2012.) The sample tested in this study had a thickness of 5 mm. Its yield strength was 389 MPa and its tensile strength was 517 MPa. The chemical composition and microstructure of this steel are shown in table 7 and figure 13, respectively. These data were taken from the inspection certificate of the tested steel sheet.

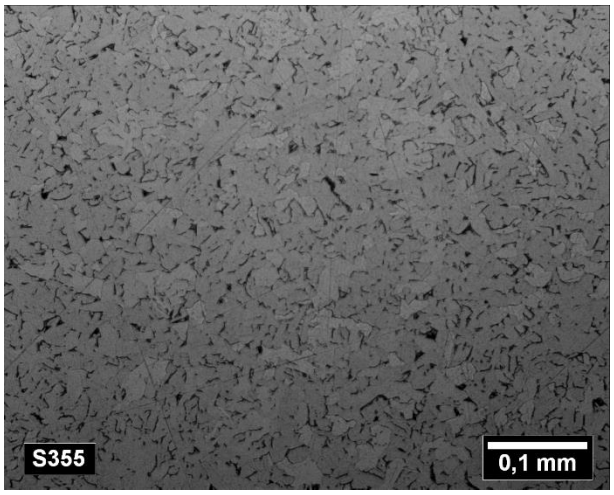

FIGURE 13. Optical microscope image of microstructure of S355 structural steel

TABLE 7. Chemical composition of structural steel S355 (wt%)

C	Si	Mn	P	S	Al	Nb	V	Cu	Cr	Ni	Mo
0,13	0,22	1,44	0,018	0,008	0,032	0,010	0,006	0,010	0,02	0,03	0,001

4.4 Manufacturing of test samples

The manufacturing process of the samples consisted of the selection and preparation of substrates, the preparation of the coating materials and the application of these materials on the substrates. Three different kinds of samples were made of each polymer-based coating; one for each type of test, i.e., adhesion strength, slurry erosion resistance and abrasion resistance tests. The manufacturing process steps are described in the following chapters.

4.4.1 Substrate selection and surface preparation

First of all, substrates for the coatings were selected and the surfaces were properly prepared. Different substrates were used for the different types of test samples. The substrate used for adhesion strength test samples was mild steel (S355). The steel sheet was cut into a rectangular shape of 200 mm long and 45 mm wide. The substrate used for abrasion test samples was a 1,4 mm Al-sheet with anodized surface coating. The substrate was cut into a circular shape of 100 mm in diameter and a hole was drilled in the center of the sample so it could be properly fastened to the threaded center post of the specimen holder of the Taber test instrument. For erosion test samples mild steel was used as substrate with a thickness of either 1 mm (for Belzona 1811 and ARC MX1 samples) or 3 mm (for Belzona 2121 and ARC BX2 samples). The substrate was cut into a rectangular shape of 160 mm long and 35 mm wide, which after casting would be cut into squares with a 35 mm side.

The surfaces of the substrates were prepared once the substrates were cut. Proper surface preparation is critical to the long-term performance of the coatings. Surface preparation included grit blasting, which was performed in order to roughen the metal surface to ensure the adhesion of polymer coatings to the substrate. The abrasive particles used for grit blasting were fresh brown fused alumina particles (NK F 020). These alumina particles, which are shown in the micrograph in figure 14, have an angular shape and an average particle size of 850 – 1180 µm. Figure 15 shows the grit blasted surface of S355 steel examined with microscope, where the rough morphology of the surface can be appreciated. After grit blasting, substrates were washed with water and soap, and then flushed with acetone.

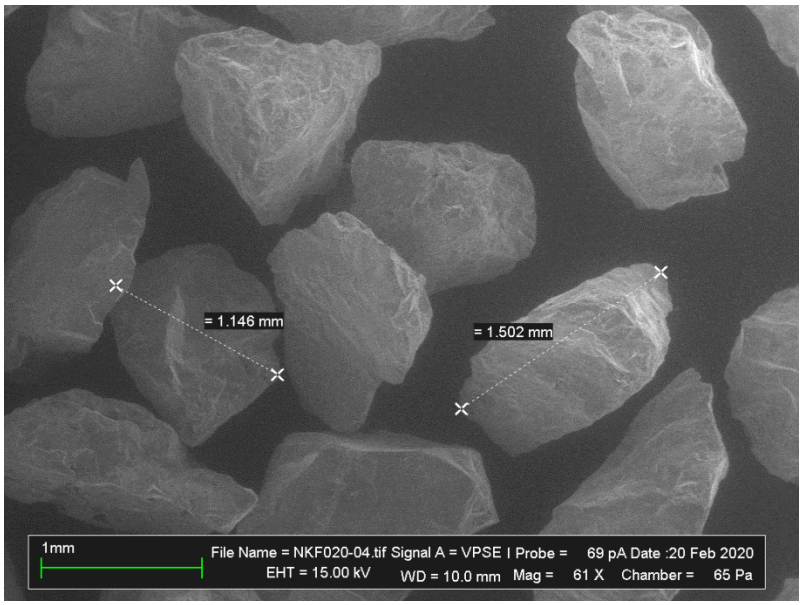

FIGURE 14. SEM micrograph of grit blasting particles (alumina particles NK F 020) showing that the maximum diameter of particles is around 1,5 mm. Magnification: 61x.

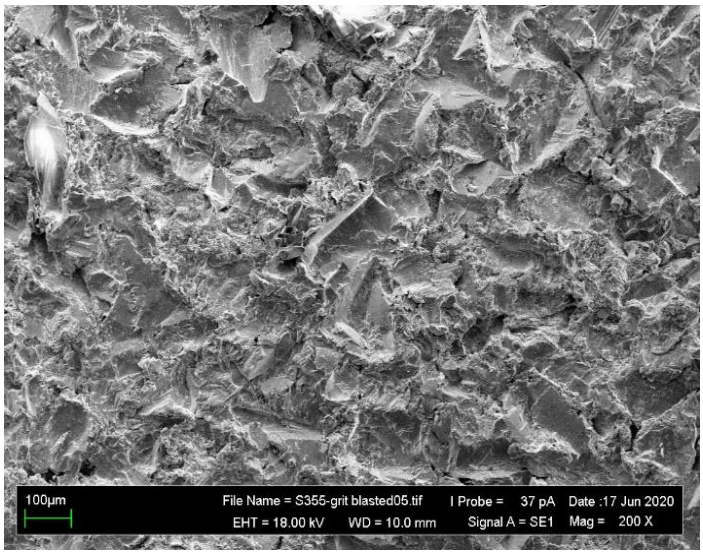

FIGURE 15. SEM micrograph of grit blasted surface of S355 structural steel. Magnification: 200x.

4.4.2 Coating preparation

Once the substrates were ready, the coating materials were prepared at room temperature. Different components needed to be mixed in order to create the composites. The components were measured with an accurate scale (~0,1 g), and then they were mixed following carefully the instructions given by the material suppliers. The applied mixing ratios by weight of the different polymer-based composites were the following:

- Belzona 1811 (base : solidifier) → 8,5 : 1.
- ARC MXP Primer (A : B) → 4,8 : 1. ARC MX1 (A : B : C) → 3,3 : 1 : 22,6.
- Belzona 2121 (base : solidifier) → 3,1 : 1.
- ARC BX2 (A : B) → 4 : 1.

FIGURE 16. Left: ARC MX1 after the mixing of all three components. Right: Belzona 1811 after mixing components.

Components were thoroughly mixed until a homogeneous color with no streaks was achieved. Figure 16 shows ARC MX1 and Belzona 1811 components being mixed. In that image the consistency of the coating materials can be seen.

4.4.3 Coating application

Once the substrates were prepared and mixtures were ready, the casting process started. First, plastic band collars were set on the substrates to delimit the casting area as shown in figure 17. Then, the mixtures were applied on the surface of the substrates using the plastic applicator that came with the materials, pressing the mixtures onto the surfaces firmly to remove air and to ensure proper adhesion. Once the materials were placed, they were smoothed to achieve the desired profile with a uniform thickness.

FIGURE 17. ARC MX1 tests sample for adhesion test after the application of the pre coating layer

ARC MX1 required the previous application of ARC MXP Primer (FIGURE 17). ARC MX1 was applied immediately after the application of a thin layer of ARC MXP Primer. The mixing and application of ARC MX1 material was somehow difficult or troublesome since it was very viscous after all reinforcement particles were added to the mix. Apparently, the number of reinforcement particles was adjusted to be as high as possible. It seemed also that ARC MX1 leaves voids or porosity quite easily to final coating, due to the non-existent flowability of the mix.

Belzona 2121 required the application of several layers to achieve the target thickness, i.e., 3 layers were applied on the adhesion test sample, 4 layers on the abrasion test sample and 3 on the erosion test sample. Belzona 2121 tests samples for adhesion tests were pretreated with Belzona 2911 conditioner to improve adhesion strength. This pretreatment was not made for other samples with Belzona 2121.

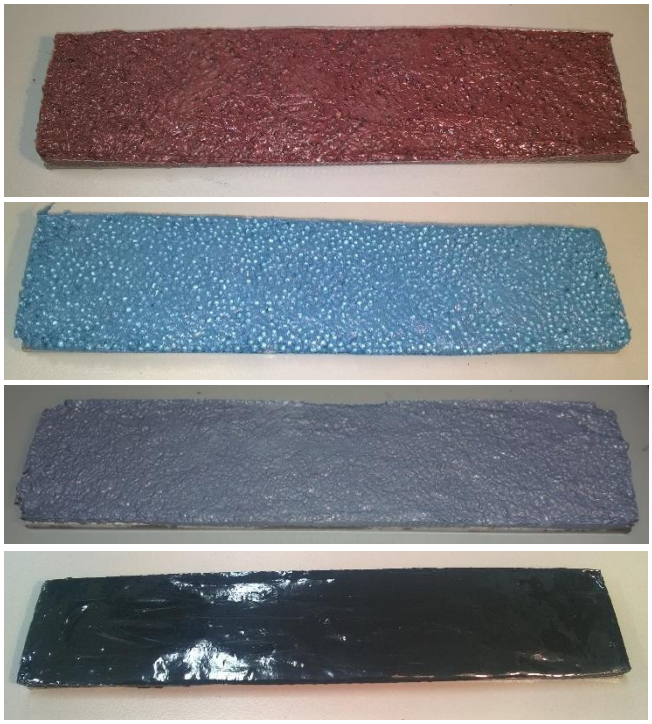

FIGURE 18. Adhesion test samples after casting. From up to down: Belzona 1811, Chesterton ARC MX1, Chesterton ARC BX2, and Belzona 2121

Some properties of all the samples are presented in table 8. As the table shows, different thicknesses were selected depending on the coating material and on the test type. The sample shape and size depended exclusively on the test type; circular shape for abrasive wear tests, long rectangular shape for adhesion tests, and smaller rectangular shape (which after casting would be cut into squares) for erosive wear tests. The adhesion test samples after casting are shown in figure 18.

TABLE 8. Coating dimensions (in mm and mm^2)

		Adhesion strength test		Abrasion resistance test	Erosion resistance test
Belzona 1811	Target thickness, mm	7	7	7	6
	Coating dimensions, mm	□ 200 x 45	□ 200 x 40	Outer ø 100 Inner ø 45	□ 160 x 35
	Coated area, mm^2	9000	8000	6264	5600
ARC MX1	Target thickness, mm	7	7	7	7
	Coating dimensions	□ 200 x 45	□ 200 x 45	Outer ø 100 Inner ø 45	□ 160 x 35
	Coated area, mm^2	9000	9000	6264	5600
ARC BX2	Target thickness	3	3,8	3	3,8
	Coating dimensions	□ 200 x 46,6	□ 200 x 45	Outer ø 100 Inner ø 45	□ 160 x 35
	Coated area, mm^2	9320	9000	6264	5600
Belzona 2121	Target thickness, mm	3	3	3	3
	Number of layers	3	3	4	3
	Coating dimensions, mm	□ 210 x 43	□ 204 x 38	Outer ø 100 Inner ø 45	□ 160 x 35
	Coated area, mm^2	9030	7752	6264	5600

4.4.4 Final modifications of test samples

All the epoxy-ceramic and polyurethane coating samples were ground to flat once they were fully cured; epoxy-ceramic samples with Ø110 mm diamond wheel (Kaindl Diamant) and polyurethane sample with a belt grinder using a P80 band. In addition, for abrasion (Taber) tests the final grinding of epoxy-ceramic and polyurethane sample surface was made with P220 diamond grinding plate (Akasel Aka-Piatto 220).

The adhesion test samples were grit blasted with alumina particles (FIGURE 14) after grinding. After this, annular holes were drilled to separate the Ø20 mm test area. The cuts were made all the way to the

substrate using a Ø25 mm diamond hole saw (Magnum quality tools). The purpose of isolating a specific diameter test area is to prevent a larger area of coating from being pulled away from the substrate, resulting in a higher pull-off pressure (DeFelsko 2020). Then, dollies with a diameter of 20 mm were grit blasted with the same alumina particles, and they were properly cleaned and glued on the top of each isolated circular Ø20 mm coating area. Dollies were glued with Araldite® AW4858/Hardener HW4858, a two-component epoxy adhesive system that seemed to be the strongest structural adhesive at the market. According to the specification, this glue shows a lap shear strength (ISO 4587) of over 35 MPa metal-to-metal joints of aluminum (Araldite specification). After gluing, samples were placed into an oven at 40 ºC. According to the glue manufacturer, performances can be enhanced by post-curing at elevated temperature. After a curing time of about 16 hours, adhesion test samples were ready to be tested (FIGURE 19).

FIGURE 19. Adhesion test samples with dollies. From up to down: Belzona 1811, Chesterton ARC MX1, Chesterton ARC BX2 and Belzona 2121

The erosion test samples were cut to square shape of 35 mm side (FIGURE 20) after they were ground to flat and so that the total thickness (substrate + coating) of all samples was 6 mm. Edge protection was required since edge wear is more dominant with larger abrasives. Edge protection was done with window plates having a 33 × 33 mm opening, as shown in figure 26.

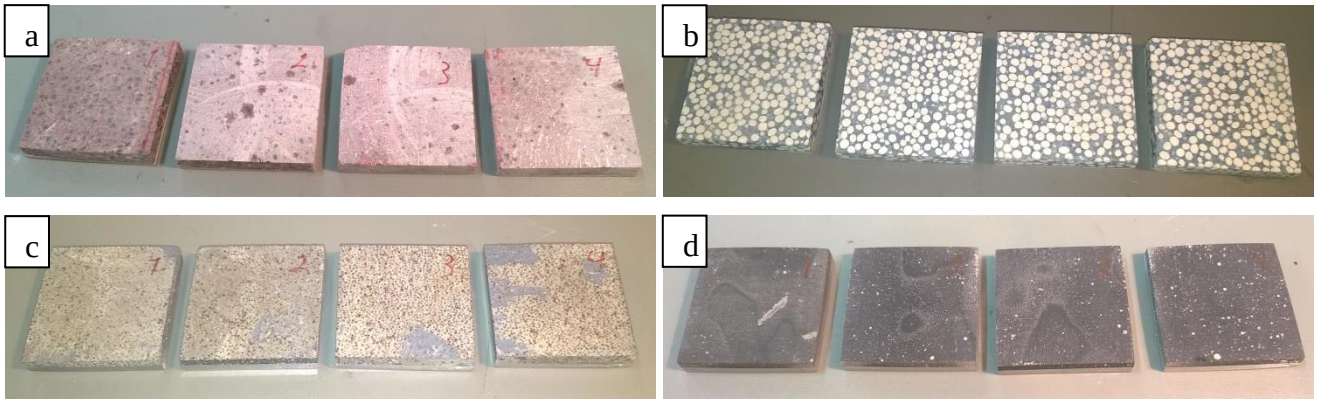

FIGURE 20. Slurry-pot test samples: (a) Belzona 1811, (b) Chesterton ARC MX1, (c) Chesterton ARC BX2, and (d) Belzona 2121

4.4.5 Metal materials samples

For the abrasion test samples, the 5 mm thick steel sheets (S355 and Raex 400) were cut into squares of 100 mm x 100 mm and were not ground. The Ni-Hard test sample surface was machined to flat. Holes were drilled in the center of the samples so they could be properly fastened to the threaded center post of the specimen holder of the Taber test instrument.

For erosion test samples (FIGURE 21), the S355 and Raex 400 steel sheets were cut into squares with 35 mm sides and ground with a belt grinder using a P80 band. Surfaces of Ni-hard samples were machined to final dimensions.

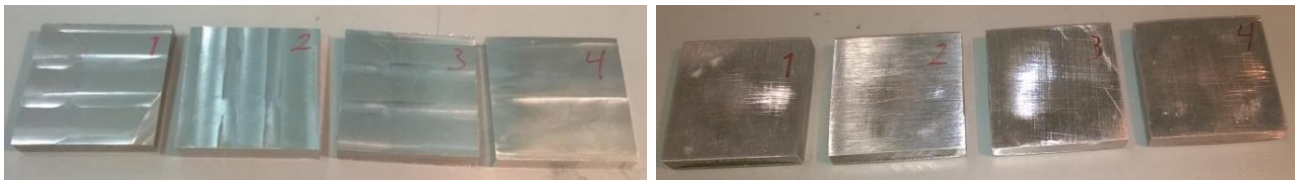

FIGURE 21. Erosion test samples of metal materials. Left: Ni-Hard. Right: S355 Steel.

4.1 Examination of the microstructure

In order to examine and analyse coating microstructure, a cross-section was prepared from each test sample. A piece of coating was mounted in two-component methacrylate resin and the cross-section surface was ground with a final grinding phase being 1 µm diamond slurry and a cloth. Examination of cross section surfaces were made both with optical microscope and with scanning electron microscope (SEM) equipped with energy dispersive X-ray spectroscopy (EDS).

In SEM-EDS method, solid surface is irradiated, or scanned with an electron beam. In SEM the image from the surface is produced based on emission or reflection of electrons from the surface. The electron beam also causes the excitation of the atoms on the surface, which emit specific wavelengths of X-rays that are characteristic of the atomic structure of the elements. An energy dispersive detector collects and analyses these X-ray emissions, providing the elemental composition of the specimen surface. (Ebnesajjad 2014, 50.) In this study, EDS analysis was used to detect the elemental compositions of various individual points in the cross-section of the coatings as well as to produce elemental distribution maps in a specific area of the cross-sections.

It is important to mention that the accuracy of quantitative EDS analysis method is rather low, and this applies especially to light elements carbon and oxygen. In addition to the inaccuracy of this method, it should also be taken into account that values for carbon are exaggerated, since the polymer matrix contains plenty of carbon.

4.2 Adhesion strength test

The adhesion between the polymer coating and the metal substrate affects notably the protective properties of the coatings (Li 2015). The adhesion strength tests were carried out at Centria University of Applied Sciences (Kokkola). The adhesion tests were performed using a Positest AT-A Automatic Adhesion Tester similar to the one shown in figure 22. This portable instrument uses hydraulic pressure to measure the force required to pull a specified area of coating away from a substrate. For this purpose, aluminum dollies of the size of 20 mm are glued to the surface to be tested and the glue is allowed to cure. Then, the instrument pulls the dolly off and measures the pressure to the strength to rip off the coating from the substrate. The maximum pull-off pressure is 24 MPa. (DeFelsko 2020.)

FIGURE 22. PosiTest AT-A Adhesion test instrument (DeFelsko 2011)

Once the pull-off test is done, three types of failures can be observed when examining the coated and dolly surfaces (FIGURE 23):

- Cohesive fracture: fracture occurs within a coating layer.
- Adhesive fracture: fracture occurs at the interface between layers.
- Glue failure: visible separation of the glue from itself, the coating or dolly.

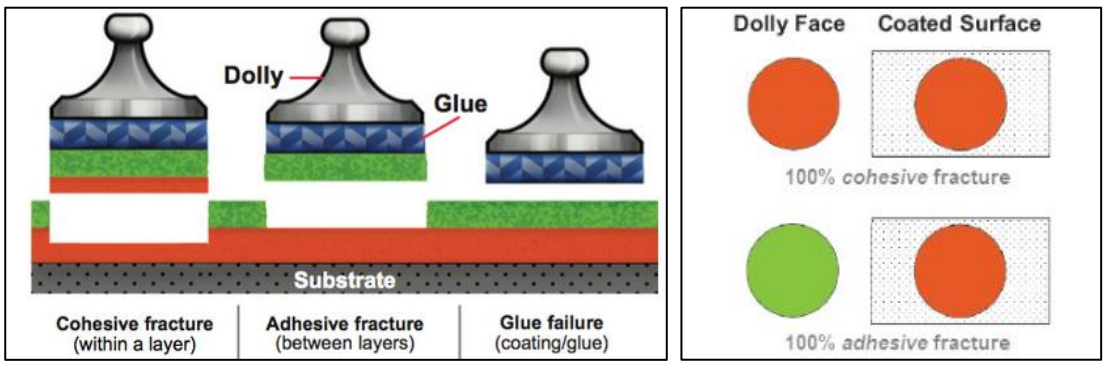

FIGURE 23. Schematic illustration of pull-off test failure types (DeFelsko 2020)

After following the steps indicated in Chapter 4.4 to manufacture the test samples of Belzona 1811, ARC MX1, ARC BX2 and Belzona 2121, pull-off tests were performed. The tests were performed at room temperature. The applied load was increased at a rate of 0,2 MPa/s. Three different types of glue had to be used for gluing the dollies to the samples. The two first glues (Loctite HY 4060 and Loctite HY4070) failed before the coating did, so the tests had to be repeated with a stronger glue (Araldite AW4858 / Hardener HW4858). The coating surfaces were ground to flat, grit blasted slightly to ensure surface roughness and cleaned with acetone before gluing the dollies, which were also grit blasted. After the gluing of dollies, adhesion test samples were cured in an oven at 40°C for 16 hours, to reach the maximum strength for Araldite AW4858 glue.

However, it turned out that it was not possible to rip off quite many of the samples with Positest instrument. Those samples were pulled off with a tensile testing machine with a setting shown in figure 24. The test was carried out with a constant speed of 0,025 mm/s.

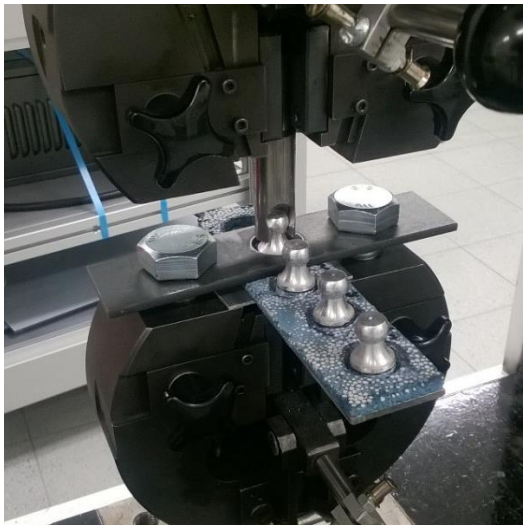

FIGURE 24. ARC MX1 sample in pull-off adhesion test in a tensile testing machine

4.3 Wear resistance tests

There are several both standardized and non-standardized wear resistance tests that can simulate different types of wear modes. The results of wear resistance tests are highly dependent on the type of wear, the type of test as well as the test parameters. Therefore, the choice of an appropriate test and parameters plays a fundamental role in measuring the wear resistance of a material. In this case, the chosen test instruments were a high-speed slurry-pot type erosion tester and a Taber abrasion tester.

4.3.1 Erosive wear resistance test

The erosive wear resistance tests were performed at Tampere Wear Center (TWC). TWC offers a wide variety of research equipment for wear testing including pin/ball-on-disk, uniaxial crusher, impeller-tumbler, high-speed slurry-pot type erosion tester, erosion tester, slurry erosion-corrosion tester, and cavitation erosion tester. Among all the available test instruments, the high-speed slurry-pot type erosion tester was a strong candidate and it was eventually chosen to measure the erosive wear resistance of the coatings (FIGURE 25a). (TWC 2019.)

The slurry-pot type erosion tester achieves high speeds up to 20 m/s with large abrasive size up to 10 mm in order to simulate slurry erosion in laboratory conditions. It consists of a pot and a motor-run rotating shaft with up to 8 wear test samples. The test samples are arranged on four different levels in horizontal positions in the so-called pin mill configuration, as shown in figure 25b. The shaft is mounted on the pot lid and the motor is connected at the end of the shaft. (Ojala, Kuokkala, Valtonen, Kivikytö-Reponen & Vuorinen 2012.) This tester enables testing of erosiveness of different abrasives, both in slurry and in dry conditions. Moreover, it is suitable for testing different materials with various sample profiles (e.g., metal bars or plates, thick and thin coatings, elastomers, and hybrid materials). (TWC 2019.)

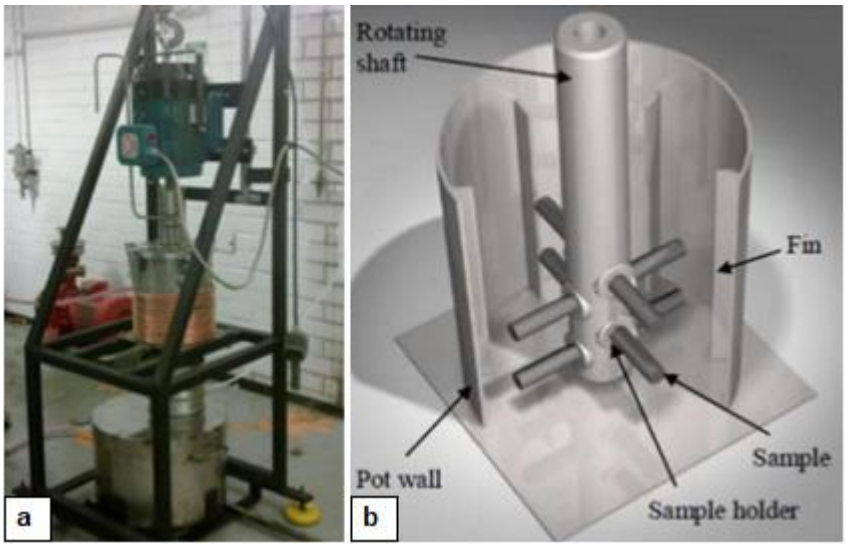

FIGURE 25. (a) High speed slurry-pot type erosion wear tester. (b) Pin mill configuration (Ojala 2017; Ojala et al. 2012)

The high-speed slurry-pot type erosion tester offers the possibility to edge protection to simulate the wear conditions in industrial slurry applications where edge wear is minimal (FIGURE 26). In a study by Ojala, Valtonen, Minkkinen and Kuokkala (2017) it was concluded that the edge wear is more dominant with larger abrasives. Also on average, the natural rubber and polyurethane showed twice as large edge effect as the steels. (Ojala et al. 2017.)

FIGURE 26. Left: High-speed slurry-pot type erosion tester. Right: edge protection (TWC 2019)

After following the steps indicated in Chapter 4.4 to manufacture the test samples, polymer-based composites Belzona 1811, ARC MX1, ARC BX2 and Belzona 2121 as well as Ni-Hard cast iron, wear-resistant steel Raex 400 and structural steel S355 were tested with this slurry-pot type erosion tester. Test settings were the same as in the study by Ojala et al. (2017). Slurry consisted of 9 wt% of coarse granite particles in the range of 8 mm to 10 mm in water, rotation speed of 1500 rpm (14 m/s in the tip of the sample), samples were in the angle of 45° in relation to the motion, and testing time was 30 minutes. Two samples of each test material were tested.

4.3.2 Abrasive wear resistance test

Abrasive wear resistance tests were carried out at Centria University of Applied Sciences (Kokkola). The tests were performed using a Taber rotary platform abrasion tester (Model 5135) also known as Taber abraser (FIGURE 27). This test is used by some of the manufacturers of epoxy-ceramic materials to define their wear resistance. The effectiveness of the wear of this instrument is milder compared to the slurry pot test.

The Taber abraser is used to test the abrasion resistance of a wide variety of materials, e.g., painted surfaces, electroplated surfaces, textile fabrics, coatings, metals, stone, ceramics, paper, glass, plastics, leather, and rubber. The Taber abraser consists of a turntable platform, where the sample is mounted, and two Taber abrasive wheels, which are lowered onto the sample surface at a specific pressure. As the platform rotates at a fixed speed, rub-wear action is produced due to the relative motion between the sample and the wheels. This abrasive wear creates a circular band mark of about 300 mm^2 on the sample surface, as shown in figure 28. The Taber abraser offers speed control options of 60 rpm and 72 rpm, it

enables testing in dry and wet conditions, and it contains precision stainless steel weights of 250 and 750 g that combined with the abraser arm provide a total load of 500 and 1000 g, respectively. (Taber rotary abraser 2020.)

FIGURE 27. Taber rotary platform abrasion tester

Belzona 1811, ARC MX1, ARC BX2 and Belzona 2121 coatings were tested with this Taber abraser. In addition, Ni-Hard cast iron, wear-resistant steel Raex 400 and structural steel S355 were also tested and used as reference materials. The abrasion resistance test was performed at room temperature, in wet conditions. Test samples of a size of ∅ 100 mm or 100 x 100 mm with a substrate thickness of few millimeters (see Chapter 4.4 for more details) were fixed into the specimen holder and then submerged in water. A load of 1000 g was applied. H10 Calibrade wheels were used. These non-resilient, vitrified wheels are designed to evaluate steel and ferrous alloys for resistance to abrasion (Genuine Taber Abrading Wheels 2020). Each sample was tested for a total of 5000 cycles at a rotating speed of 60 rpm. The wheels were refaced between each 1000 rounds, at the same time when the sample was weighed. This refacing was made by placing a coarse ∅110 mm diamond grinding wheel (Kaindl Diamant) to the (dry) specimen stage and the stage was rotated a total of 50 rounds. It turned out that without this resurfacing, the wheel surface became clogged with epoxy and it seemed to lose its abrasive properties.

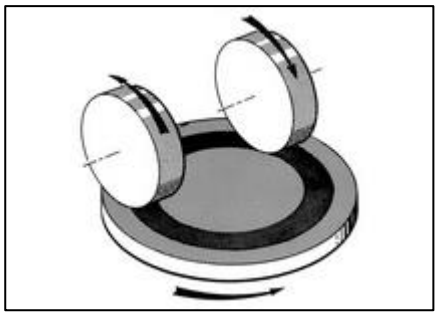

FIGURE 28. Schematic diagram of Taber abraser (Taber rotary abraser 2020)

The method used to measure wear involved direct determination of the amount of removed material as mass loss. Taber Wear Index was also calculated. This index indicates the rate of wear and is calculated by measuring the loss in weight per thousand cycles of abrasion. The lower the wear index, the better the abrasion resistance.

$$I = [(A - B) \cdot 1000] / C \quad (1)$$

where I is the wear index, A is the weight in milligrams of specimen before abrasion, B is the weight in milligrams of specimen after abrasion and C is the number of test cycles. (Taber rotary abraser 2020.)

5 RESULTS AND DISCUSSION

The findings of the present study and the discussion about these findings are presented in this chapter. The chapter is divided in four sections: SEM/EDS results, adhesion strength test results, slurry-pot type erosion test results and Taber abrasion test results.

5.1 Coating microstructure

The structures of the epoxy-ceramic coatings as well as the polyurethane-based coating were first examined from the cross-section with an optical microscope. The optical microscope images of the cross-sections show how the reinforcement particles of the different coating materials differ from each other:

- Belzona 1811 contains large angular dark particles (FIGURE 29a),
- ARC MX1 contains large spherical white particles and small dark particles (FIGURE 29b),
- ARC BX2 contains small spherical dark particles (FIGURE 29c), and
- Belzona 2121 is an unreinforced coating; it seems to contain porosity and delamination of coating layers (FIGURE 29d).

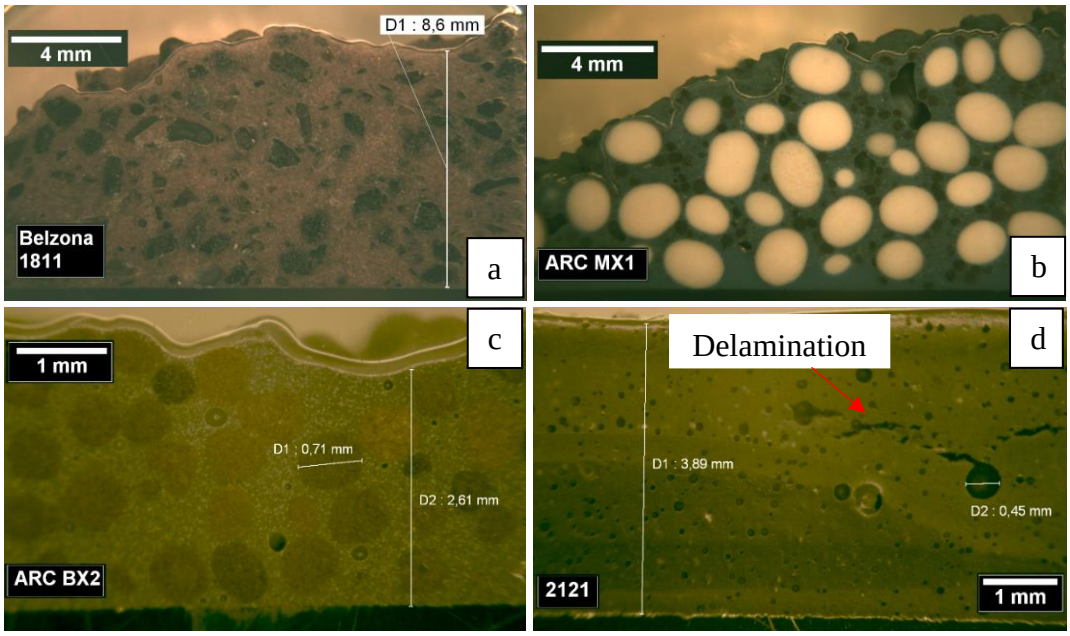

FIGURE 29. Optical microscope images of cross-section of (a) Belzona 1811 coating, (b) ARC MX1 coating, (c) ARC BX2 coating and (d) Belzona 2121 coating. Note the varying magnification between images.

A Vickers hardness test was performed to cross-section surface to measure the hardness of the reinforcement particles of epoxy-ceramic samples Belzona 1811, ARC MX1 and ARC BX2. The hardness of epoxy matrix was not measured. The hardness of elastic, polyurethane-based material Belzona 2121 was measured with a Shore A method from the ground surface of adhesion test samples. The results are shown in figure 30 and table 9.

TABLE 9. The size and hardness of the reinforcement particles of the different coatings

Coating name	Coating type	Reinforcement size	Reinforcement hardness (HV1*)	Reinforcement nature	Matrix hardness (Shore A)
Belzona 1811	Epoxy-ceramic	Max: ~1,3 mm	Min: 1406 Max: 1648 Aver: **1527**	Very brittle	-
ARC MX1	Epoxy-ceramic	Max: ~2,2 mm	Min: 540 Max: 1050 Aver: **808**	Tough	-
ARC BX2	Epoxy-ceramic	Max: ~0,8 mm	Min: 552 Max: 912 Aver: **776**	Tough	-
Belzona 2121	Polyurethane	< 10 μm	-	-	Min: 84 Max: 91 Aver: **89**

**HV1 = 1 kg load force*

The hardness of Belzona 1811 ceramic particles was difficult to measure due to their brittleness. Several measurements were omitted since particle fragmented and it was not possible to measure indentation. In fact, this 1 kg weight was chosen because the particles in Belzona 1811 coating fractured with higher measurement weights. The fractures caused by the indenter in this material can be observed in figure 30. On the other hand, ARC MX1 and ARC BX2 reinforcement particles showed a tough nature. Average hardness of Belzona 1811 reinforcement (1527 HV1) almost doubled that of ARC MX1 (808 HV1) and ARC BX2 (776 HV1).

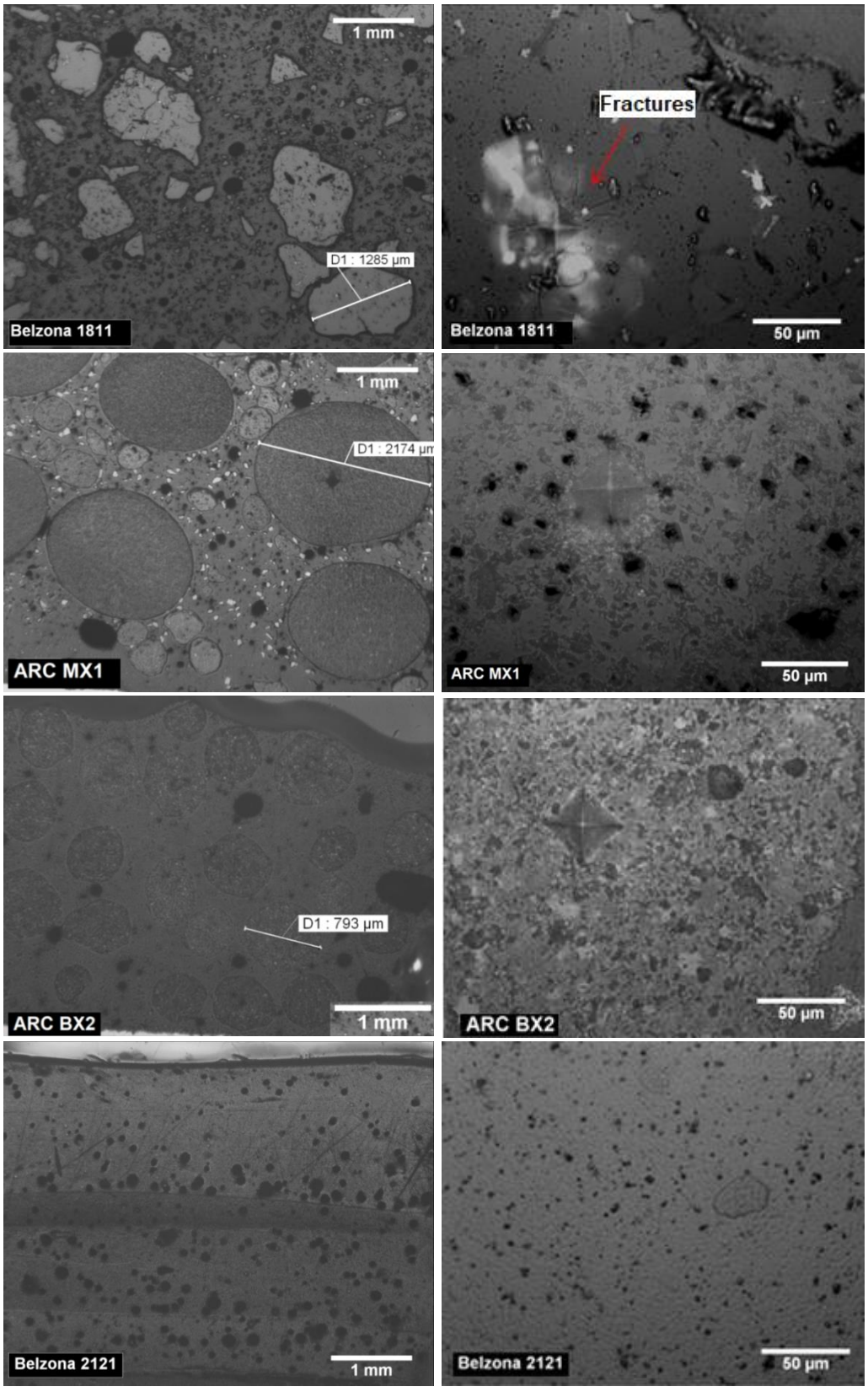

FIGURE 30. Optical microscope images of cross-sections of the studied composite coatings. On the left: low magnification to show reinforcement particle size. On the right: higher magnification to shown Vickers indentations on the reinforcement particle surface (1811, MX1 and BX2).

5.1.1 Belzona 1811 coating

Figure 31 shows SEM images of the cross-section with marked points of EDS-analyzed positions. The results of the EDS analysis are shown in table 10 and the elemental maps are shown in figure 32.

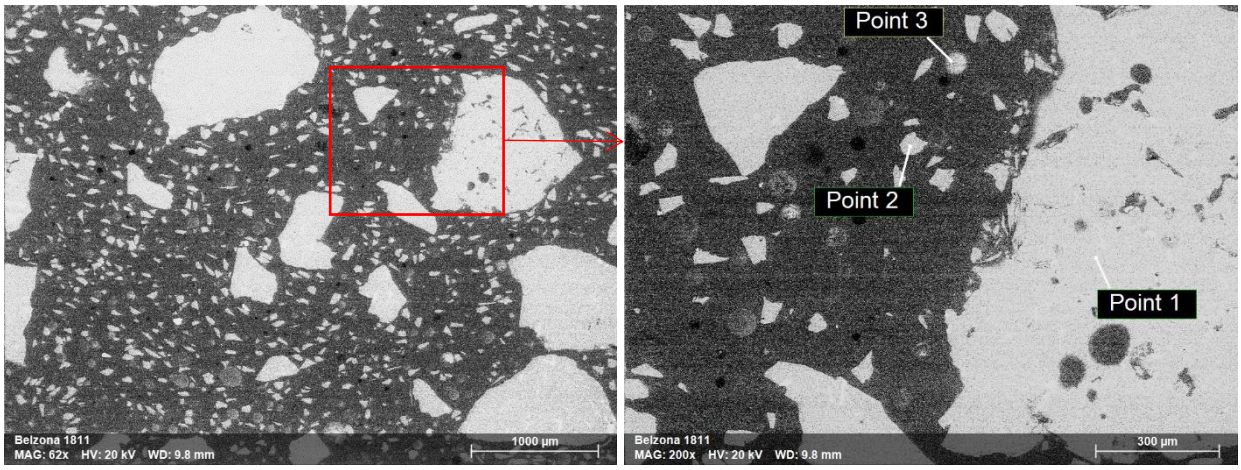

FIGURE 31. SEM images of Belzona 1811 coating cross-section with marked points of EDS-analyzed positions. Magnifications: left: 62x, right: 200x.

TABLE 10. EDS analysis results of three specific points in Belzona 1811 cross-section (at%)

Belzona 1811	C	O	Al	Si	S	Ti	Fe	Ni
Point 1	43	**36**	**20**	0,1		0,3		
Point 2	42	**40**	**18**	0,2	0,1	0,1	0,1	
Point 3	**66**	**14**	**5,4**	1,0	0,4	0,1	**13**	0,2

The results of the microstructure examination presented in this chapter show that Belzona 1811 contains large angular particles with a maximum diameter of 1,3 mm. These particles consist mainly of aluminum (Al) and oxygen (O). Belzona 1811 also contains smaller particles, some of them consist mainly of aluminum (Al) and oxygen (O), and others also contain iron (Fe).

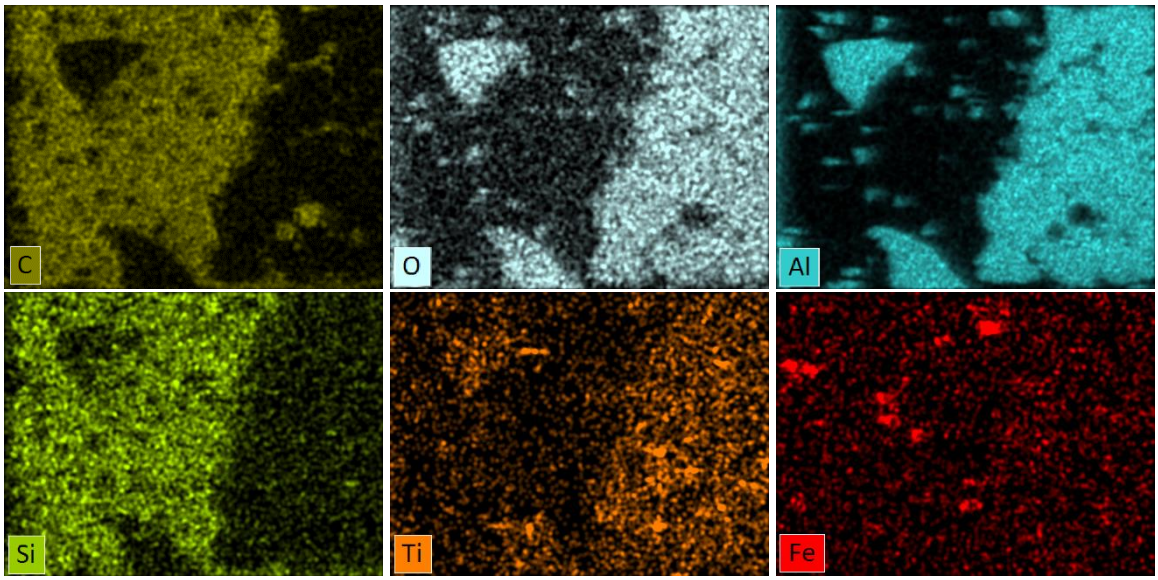

FIGURE 32. SEM/EDS elemental distribution maps in cross-section of Belzona 1811 sample. Magnification 200x.

5.1.2 ARC MX1 coating

Figure 33 shows the SEM images of the cross-section with marked points of EDS-analyzed positions. The results of the EDS analysis are shown in table 11 and the elemental maps are shown in figure 34.

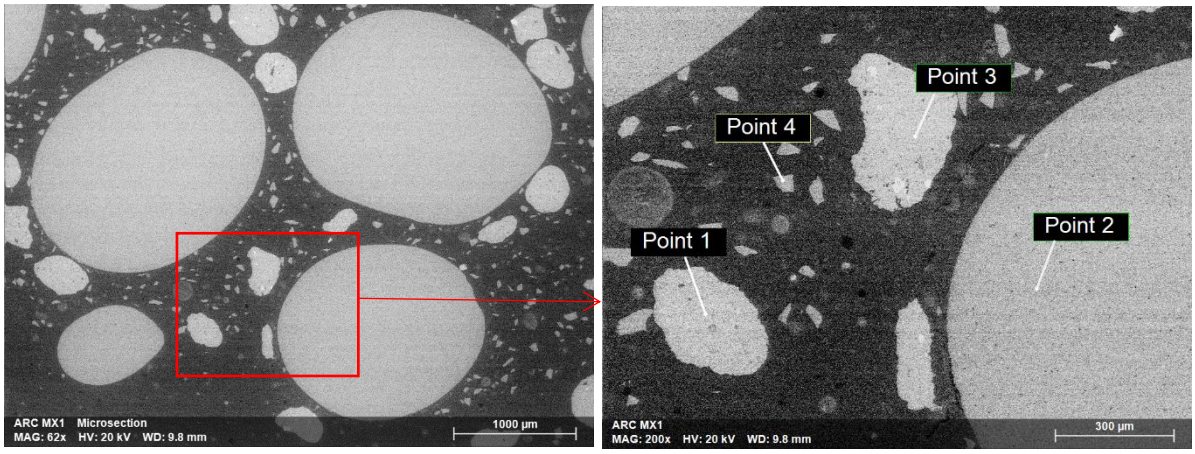

FIGURE 33. SEM images of ARC MX1 coating cross-section with marked points of EDS-analyzed positions. Magnifications: left: 62x, right: 200x.

TABLE 11. EDS analysis results of four specific points in ARC MX1 cross-section (at%)

MX1	C	O	Mg	Al	Si	K	Ca	Ti	Fe
Point 1	29	**47**		**20**	1,3	0,1	0,4	0,5	**2,9**
Point 2	20	**50**	3,3	**25**	1,1		0,4		0,3
Point 3	31	**46**		**17**	1,4	0,1	0,4	0,9	**3,3**
Point 4	**65**	10		1,6	**23**				0,3

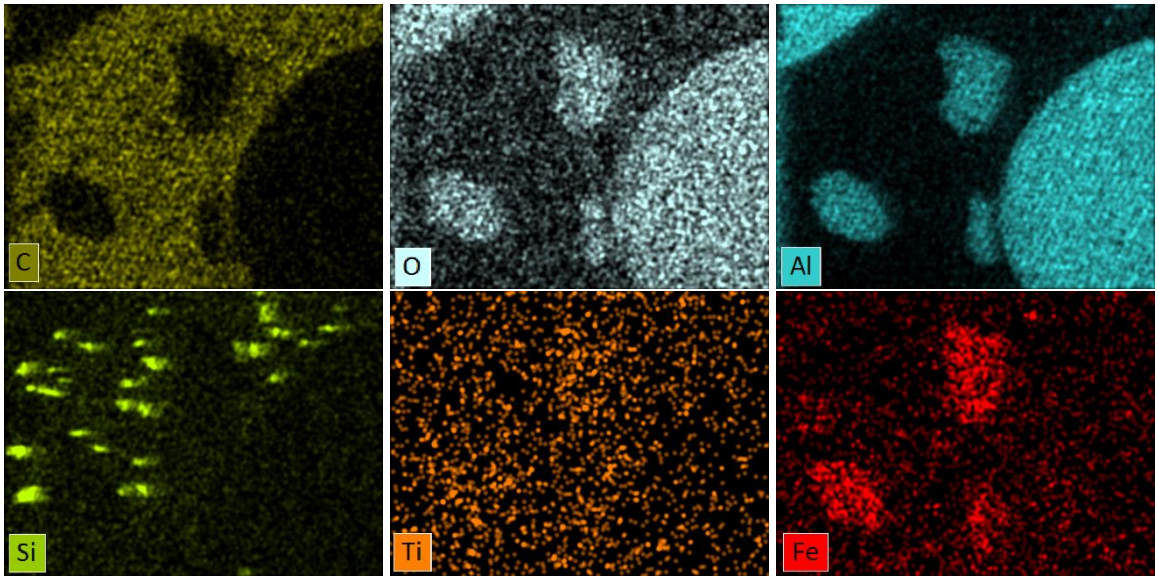

FIGURE 34. SEM/EDS elemental distribution maps in cross-section of ARC MX1 sample. Magnification 200x.

The results of the microstructure examination presented above show that ARC MX1 contains white spherical or oval particles with a maximum diameter of 2,2 mm. These large particles consist mainly of aluminum (Al) and oxygen (O). It also contains smaller particles that consist mainly of aluminum (Al) and oxygen (O), but also iron (Fe). There are also even smaller particles consisting mainly of carbon (C) and silicon (Si).

5.1.3 ARC BX2 coating

Figure 35 shows the SEM image of ARC BX2 coating cross-section with marked points of EDS-analyzed positions. The results of the EDS analysis are shown in table 12 and the elemental maps are shown in figure 36.

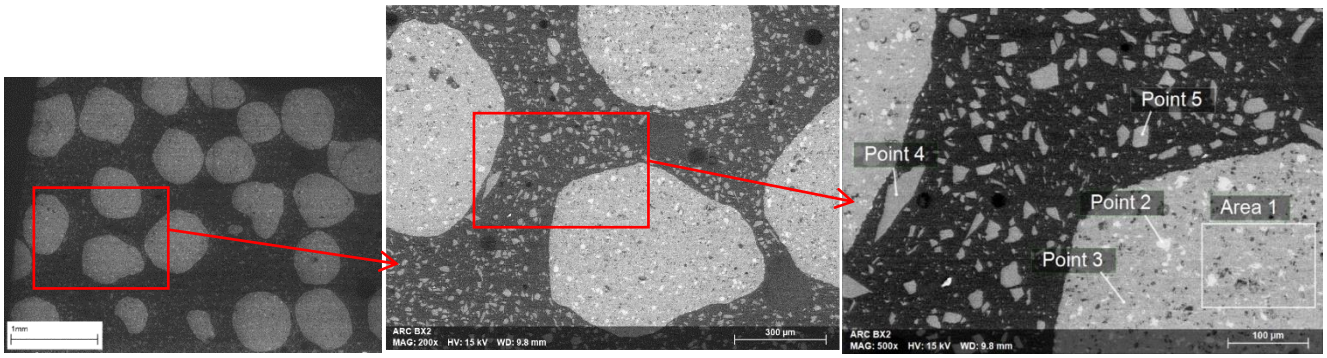

FIGURE 35. SEM image of ARC BX2 coating cross-section with marked points of EDS-analyzed positions. Magnifications: left: 65x, middle: 200x, right: 500x.

TABLE 12. EDS analysis results of a specific area and four points in ARC BX2 cross-section (at%)

ARC BX2	C	O	Na	Al	Si	K	Ca	Ti	Fe	Zr
Area 1	28	**46**		**19**	3,2			0,7	2,0	0,0
Point 2	28	**45**	0,2	**10**	2,0			**6,3**	**8,7**	0,1
Point 3	31	**45**	0,1	**19**	3,7		0,1	0,4	1,6	
Point 4	35	**44**	3,6	**5,8**	**12**			0,2	0,4	
Point 5	38	**40**	0,3	**5,7**	**12**	3,2		0,1	0,4	

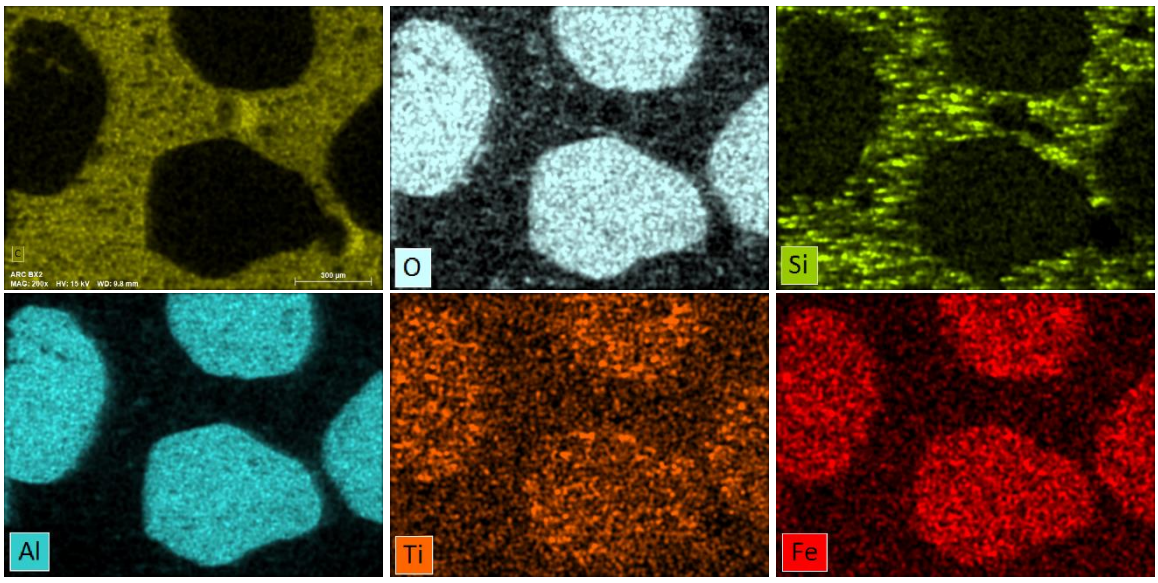

FIGURE 36. SEM/EDS elemental distribution maps in cross-section of ARC BX2 sample. Magnification 200x.

The results of the microstructure examination presented in this chapter show that ARC BX2 contains round particles that are not totally spherical, with a maximum diameter of 0,8 mm. These particles are mainly aluminum (Al) and oxygen (O), but there also some areas with iron (Fe) and titanium (Ti). ARC BX2 also contains smaller fragmented angular particles consisting of silicon (Si), oxygen (O) and aluminum (Al).

5.1.4 Belzona 2121 coating

Figure 37 shows the SEM image of ARC BX2 coating cross-section with marked points of EDS-analyzed positions. The results of the EDS analysis are shown in table 13 and the elemental maps are shown in figure 38.

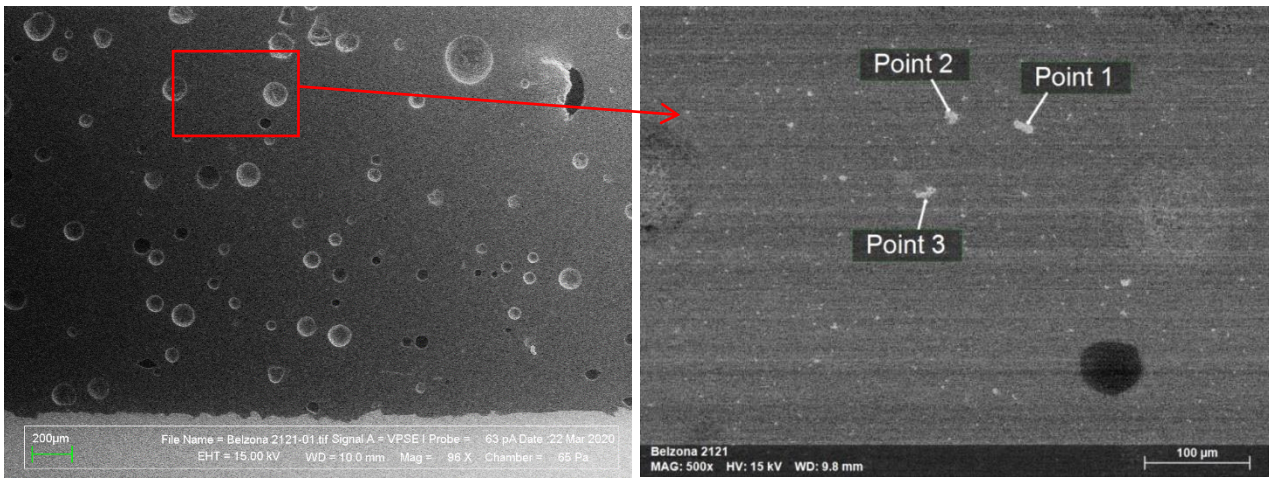

FIGURE 37. SEM image of Belzona 2121 coating cross-section with marked points of EDS-analyzed positions. Magnifications: left: 65x, right: 500x.

TABLE 13. EDS analysis results of three specific points in Belzona 2121 cross-section (at%)

Belzona 2121	C	O	Na	Al	Si	S	Cl	K	Ca	Fe
Point 1	**58**	**31**	1,7	**3,8**	**3,8**			0,7	0,4	0,2
Point 2	**50**	**37**	2,8	**4,4**	**4,7**	0,0	0,1	0,9	0,1	0,1
Point 3	**56**	**35**	0,8	**2,7**	**3,5**			0,5	0,4	0,8

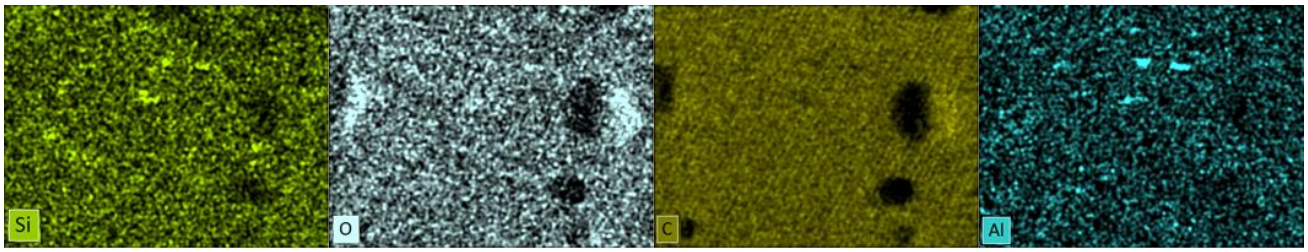

FIGURE 38. SEM/EDS elemental distribution maps in cross-section of Belzona 2121 sample. Magnification 500x.

The results of the microstructure examination presented in this chapter show that Belzona 2121 coating seems to contain some small (<20 μm) particles that contain aluminum (Al) and silicon (Si). Relatively large amount of porosity is visible in the coating (FIGURE 37).

5.2 Adhesion strength test

The results of the pull-off test are presented in table 14 and graph 1. It seemed that 20,68 MPa was the highest load that Positest tester could apply. However, those samples that did not break at a load of 20,68 MPa were tested with a tensile testing machine (FIGURE 24) and they did not seem to bear higher loads. The results obtained with the tensile testing machine are written in brackets in table 14.

TABLE 14. Pull-off adhesion test results (MPa)

Test sample	Dolly No.	Belzona 1811	ARC MX1	ARC BX2	Belzona 2121
1	1	20,68* (16,80)	20,68* (19,73)	20,68* (9,52)	7,18
	2	20,68	20,68* (20,68)	18,43	5,52
	3	19,15	20,68* (21,89)	10,76	4,27
	4	20,68* (18,71)	20,68* (19,40)	16,75	7,83
	5	20,68* (18,56)	20,43	16,24	5,57
2	1	20,68* (19,88)	20,68* (21,12)	20,68* (13,65)	3,84
	2	20,68* (16,73)	20,68* (21,52)	20,27	3,97
	3	20,68* (16,29)	20,68* (22,55)	14,01	3,95
	4	20,68* (17,86)	20,68* (19,25)	20,05	-
	5	18,81	20,68* (19,80)	18,64	5,59
Average		**20,34**	**20,66**	**17,65**	**5,30**
Min		18,81	20,43	10,76	3,84
Max		20,68	20,68	20,68	7,83

**Maximum force from Positest instrument. Dolly was not ripped off.*

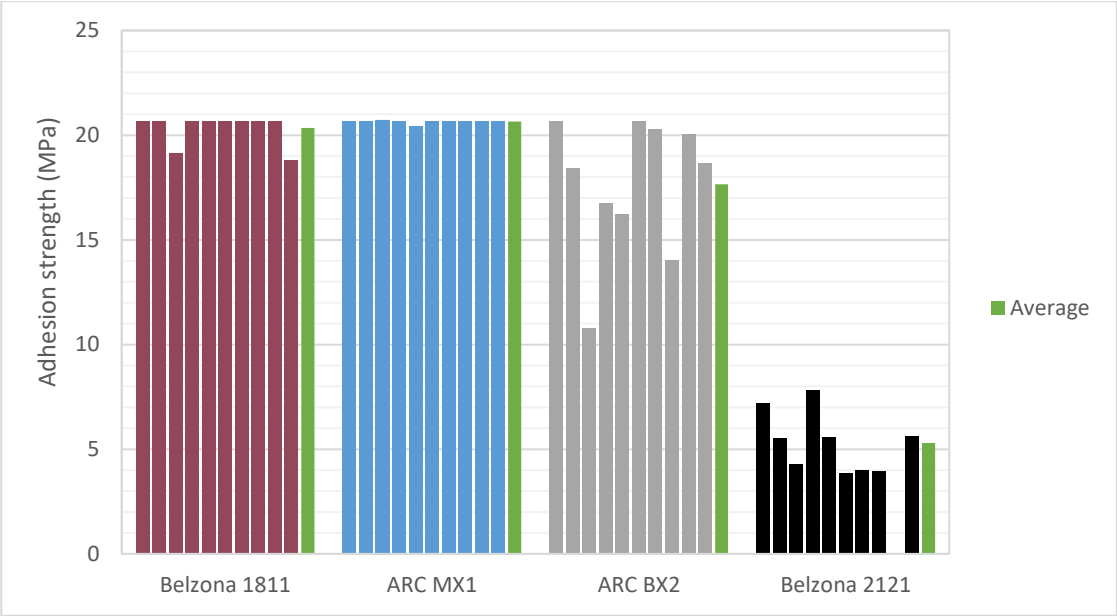

GRAPH 1. Adhesion strength test results with Positest instrument

FIGURE 39. Some of the samples after adhesion test. From up to down: Belzona 1811, Chesterton ARC MX1, Chesterton ARC BX2 and Belzona 2121

When analyzing these results, it can be observed that epoxy-ceramic coatings outperformed polyurethane-based coating. ARC MX1 epoxy-ceramic coating performed better than the rest, with an adhesion strength 3,9 times higher than that of Belzona 2121 (PU-based). Among the epoxy-ceramic coatings, ARC MX1, which was applied to the substrate after conditioning it with a primer layer, showed the strongest adhesion to the substrate, followed closely by Belzona 1811.

Different types of failures were obtained for different materials and dollies, as can be seen in figure 39. For adhesion test with Positest device, the following failures were obtained:

- Ten samples of Belzona 1811 were successfully tested: 7 samples showed no fracture (neither between the dolly and surface, nor between the steel substrate and the coating), 2 showed fracture at the middle of the coating layer, and 1 showed fracture mainly inside the coating but also some at the interface.
- Ten samples of Chesterton ARC MX1 were tested: 9 samples showed no fracture and 1 showed fracture at the middle of the coating layer.
- Nine samples of Belzona 2121 were successfully tested: some samples showed fracture mainly between the coating layers, some inside the coating but not between layers, some at the gluing of the dolly, some close to the interface and some were unclear.
- Ten samples of Chesterton ARC BX2 were tested: 4 samples showed fracture both at the interface and inside coating, 4 showed fracture mainly between the substrate and the coating, and 2 showed no fracture.

For adhesion test with tensile testing machine, the following failures were obtained:

- Seven samples of Belzona 1811 were tested: 5 samples showed fracture at the middle of the coating layer and 2 showed fracture mainly at the middle of the coating layer but a small portion at the interface.
- Nine samples of ARC MX1 were tested: 4 samples showed fracture at the middle of the coating layer, 3 showed fracture broth close to the interface and inside the coating and 2 showed fracture mainly close to the interface.
- Two samples of ARC BX2 were tested: samples showed fracture mainly close to the interface.

5.3 High-speed slurry-pot type erosion test

The results of the slurry-pot erosion test are presented in table 15. Material mass loss was measured (GRAPH 2) and then, using material densities, volume loss was calculated (GRAPH 3). Belzona 1811 experienced the highest volume loss while Ni-Hard cast iron the lowest. In general, metal materials performed significantly better than epoxy-ceramic coatings. Only unreinforced polyurethane coating Belzona 2121 showed wear resistance comparable to that of metal materials. Among the epoxy-ceramic coatings, Belzona 1811 showed a material volume loss 2,1 and 3,7 higher than that of ARC BX2 and ARC MX1, respectively. These results may be due to the nature of the reinforcement particles of these coatings. The brittleness of the reinforcement particles in Belzona 1811 was clearly evident according to the hardness measurements (TABLE 9) and, respectively, the particles in ARC MX1 seemed to be very tough.

TABLE 15. Slurry-pot test results

	mass loss (mg)	density (g/mm^3)	volume loss (mm^3)
Belzona 1811-1	1398	0,00218	641
Belzona 1811-2	1635		750
Average	**1516,5**		**696**
ARC BX2-1	757	0,0021	360
ARC BX2-2	614		292
Average	**685,5**		**326**
ARC MX1-1	483	0,0026	186
ARC MX1-2	492		189
Average	**487,5**		**188**
Belzona 2121-1	71	0,0012	59
Belzona 2121-2	59		49
Average	**65**		**54**
S355-1	183	0,0078	23
S355-2	189		24
Average	**186**		**24**
Raex400-1	233	0,0078	30
Raex400-2	115		15
Average	**174**		**22**
Nihard-1	79	0,0076	10
Nihard-2	80		11
Average	**79,5**		**10**

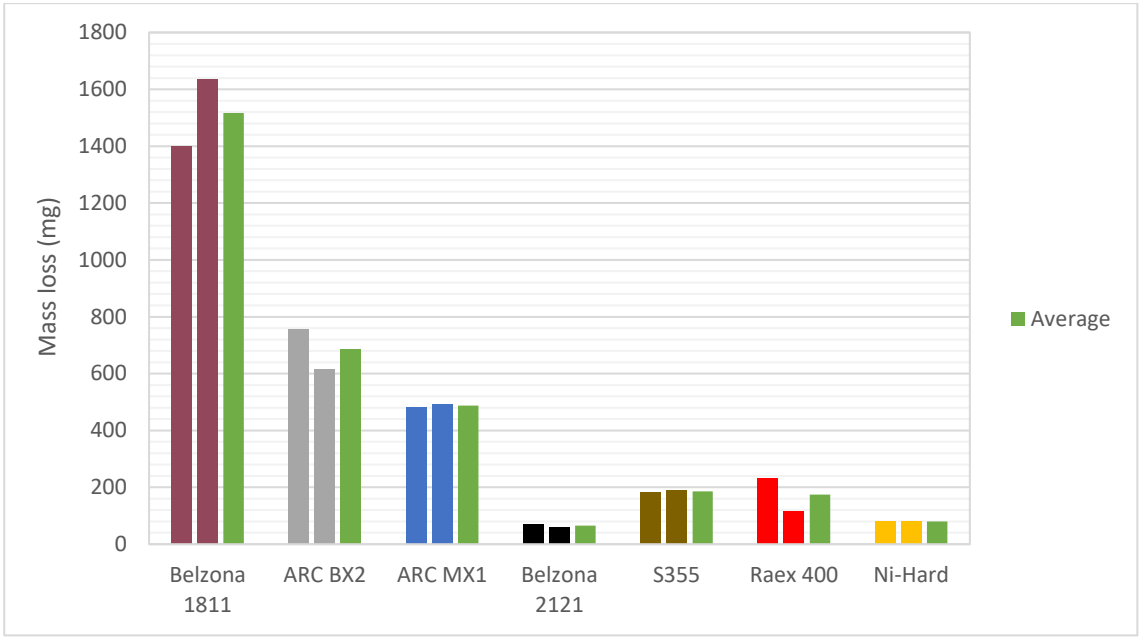

GRAPH 2. Slurry-pot erosion test results (mass loss)

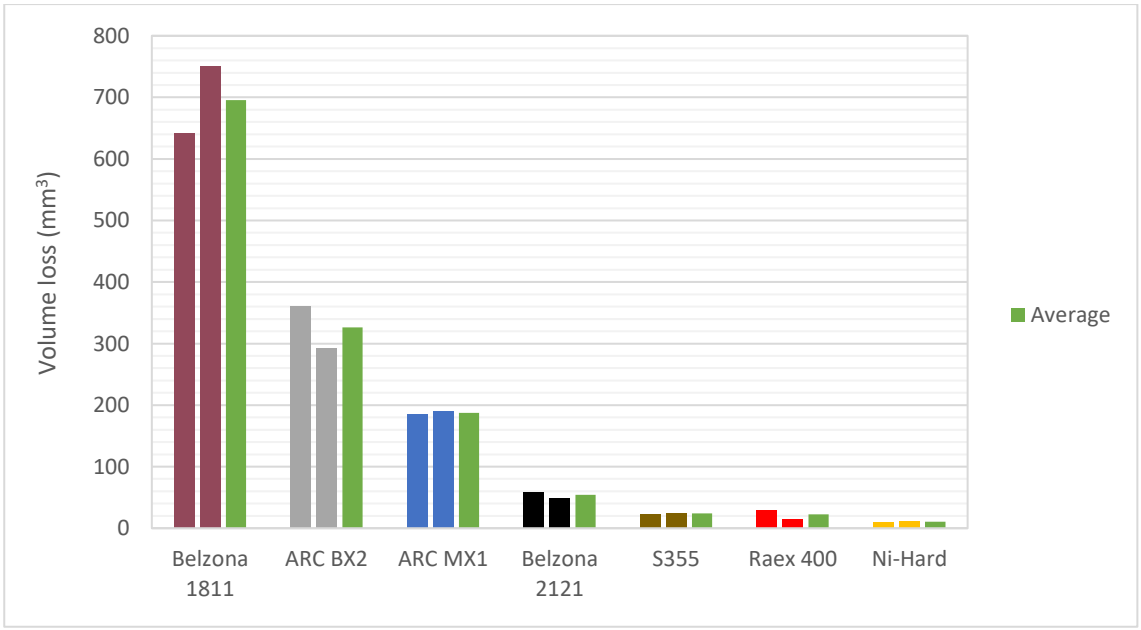

GRAPH 3. Slurry-pot erosion test results (volume loss)

Figure 40 shows the test samples of both polymer-based materials and metal materials after slurry erosion resistance test. The surface of epoxy-ceramic coating Belzona 1811, which definitely suffered the highest loss of material, showed a clear concave shape (FIGURE 40a).

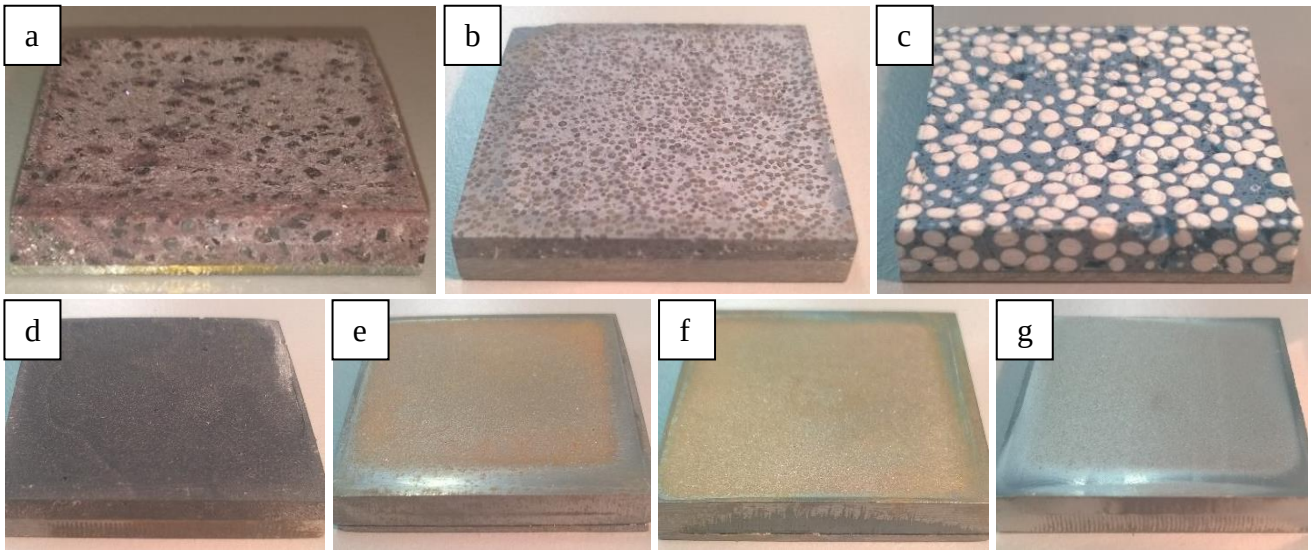

FIGURE 40. Test samples after erosion resistance test: (a) Belzona 1811, (b) ARC BX2, (c) ARC MX1, (d) Belzona 2121, (e) S355 steel, (f) Raex 400 steel, and (g) Ni-Hard cast iron

5.4 Taber abrasion test

The results of the Taber abrasion test are presented in table 16 and graph 4. Table 16 also includes Taber Wear Index values, which represent mass loss per 1000 cycles. Under the given test conditions, the wear rates of unreinforced polyurethane (Belzona 2121) were the lowest of all whereas the rates of the steels were the highest. Among the epoxy-ceramic coatings, the one containing the smallest reinforcement particles (ARC BX2) showed the highest wear rates, while ARC MX1 and Belzona 1811 showed a similar behavior. The wear rates of the epoxy-ceramic coatings Belzona 1811, ARC MX1 and ARC BX2 are, respectively, 2,1, 2,3 and 3,5 times higher than that of the unreinforced polyurethane coating Belzona 2121.

TABLE 16. Taber abrasion test results, mass loss (g)

Material \ Rev.	0	1000	2000	3000	4000	5000	Taber Wear Index
ARC MX1 (EP-Cer)	0	0,06	0,11	0,22	0,27	**0,35**	0,07
ARC BX2 (EP-Cer)	0	0,15	0,27	0,36	0,47	**0,5**	0,10
Belzona 1811 (EP-Cer)	0	0,03	0,10	0,18	0,26	**0,31**	0,06
Belzona 2121 (PU)	0	0,05	0,07	0,10	0,12	**0,15**	**0,03**
Ni-Hard cast iron	0	0,11	0,22	0,37	0,53	**0,69**	0,14
Raex 400 steel	0	0,50	0,91	1,23	1,55	**1,91**	0,38
S355 steel	0	0,43	0,84	1,19	1,57	**1,94**	**0,39**

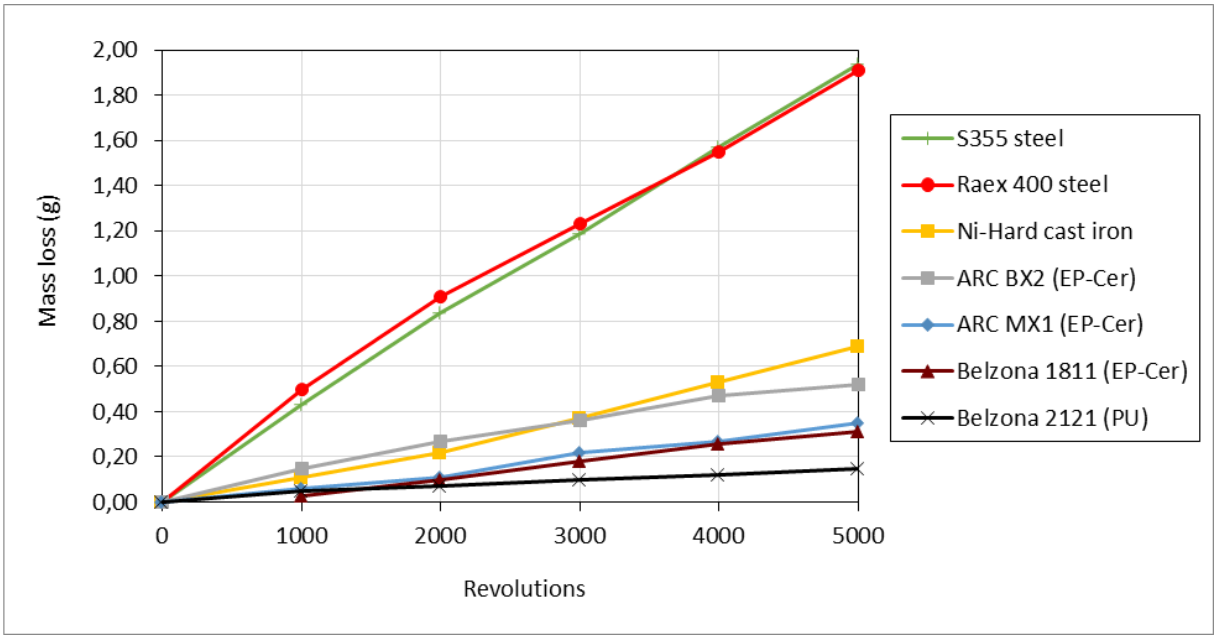

GRAPH 4. Taber test results (mass loss)

To give a true measure of the comparative wear resistance, material densities were taken into account and the loss in volume of the material was calculated. Same densities than the ones showed in table 15 were used here. The results are shown in table 17 and graph 5. Extremely abrasion resistant Ni-Hard cast iron performed the best, while steels and epoxy-ceramic coating ARC BX2 showed the highest volume losses. Among the epoxy-ceramic coatings, the one containing the smallest reinforcement particles (ARC BX2) showed the highest wear rate, while ARC MX1 and Belzona 1811 showed a similar behavior.

TABLE 17. Taber abrasion test results, volume loss (mm^3)

Material \ Rev.	0	1000	2000	3000	4000	5000	Taber Wear Index
ARC MX1 (EP-Cer)	0	23,08	42,31	84,62	103,85	134,62	27
ARC BX2 (EP-Cer)	0	71,43	128,57	171,43	223,81	247,62	**50**
Belzona 1811 (EP-Cer)	0	13,76	45,87	82,57	119,27	142,20	28
Belzona 2121 (PU)	0	41,67	58,33	83,33	100,00	125,00	25
Ni-Hard cast iron	0	14,47	28,95	48,68	69,74	90,79	**18**
Raex 400 steel	0	64,10	116,67	157,69	198,72	244,87	49
S355 steel	0	55,13	107,69	152,56	201,28	248,72	**50**

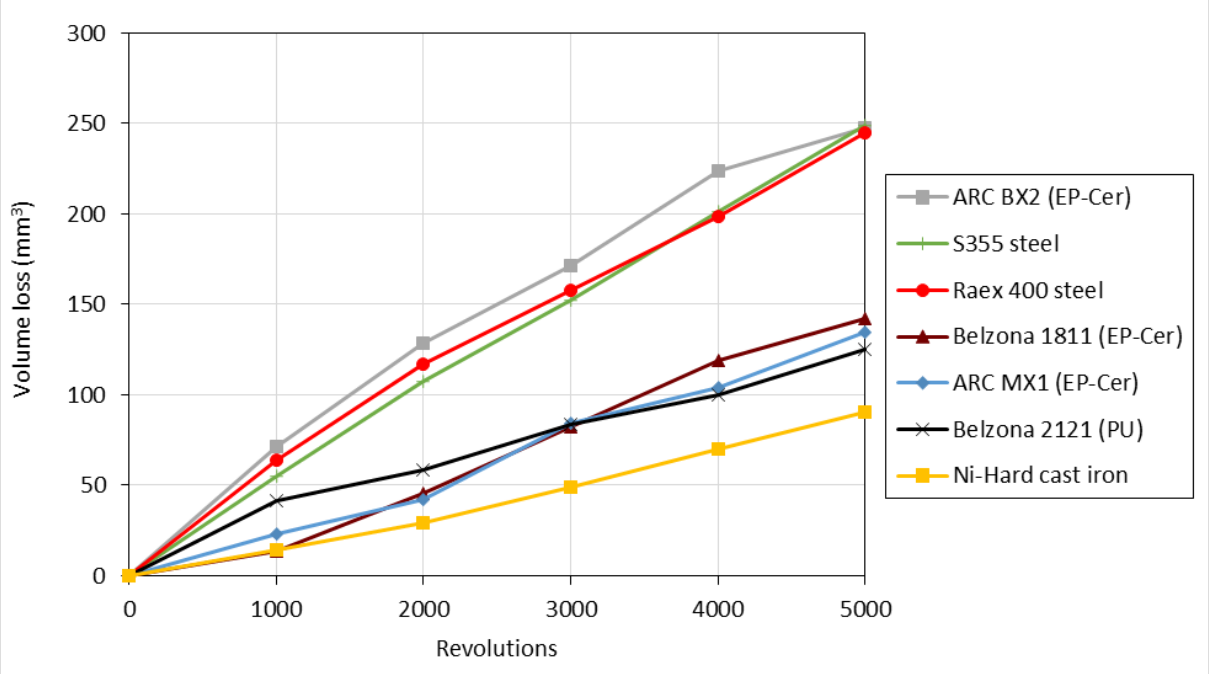

GRAPH 5. Taber test results (volume loss)

Figure 41 and figure 42 show, respectively, polymer-based samples and metal material samples after 5000 cycles in Taber abrasion test. The circular band mark made by the Taber abrasive wheels on the sample surfaces can be clearly observed in the images.

FIGURE 41. Taber samples after 5000 revolutions. From left to right: ARC MX1, ARC BX2, Belzona 1811 and Belzona 2121

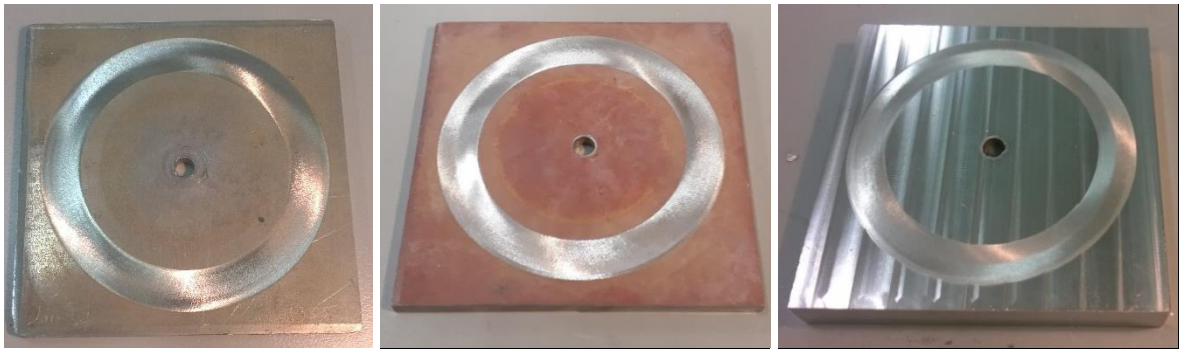

FIGURE 42. Taber samples after 5000 revolutions. From left to right: S355 steel, Raex 400 steel, and Ni-Hard cast iron

6 CONCLUSIONS

This thesis aimed to study the applicability of polymer-ceramic composite coatings to replace metallic coatings in repairing of metal components. Based on the tests performed, it can be concluded that the applicability of the studied wear-resistant coatings depends on the type of wear that they are subjected to and, hence, the component application. Both epoxy-ceramic coatings ARC MX1, ARC BX2 and Belzona 1811, as well and polyurethane-based Belzona 2121 coating performed well in Taber wear test, when the type of wear was purely sliding abrasion without any impacts. On the other hand, epoxy-ceramic coatings did not perform well under slurry erosion; their wear resistance was not at the same level compared with that of metal materials with higher toughness. Polyurethane-based Belzona 2121 coating, however, showed slurry erosion resistance comparable to that of metal materials.

Regarding the adhesion strength of these coatings to the substrate, epoxy-ceramic coatings greatly outperformed polyurethane-based coating in the pull-off adhesion test. It was also observed that conditioning the surface with a primer layer in ARC MX1 clearly improved adhesion, showing ARC MX1 the highest adhesion strength to the substrate among all the tested coatings. Polyurethane coating Belzona 2121 showed some delamination between coating layers, which was evident in adhesion tests (FIGURE 39) and in cross-section images (FIGURE 30). However, this did not seem to affect the wear resistance tests.

Regarding the application of these coatings to the substrate, it was relatively easy and did not require any special skill or equipment. Among all the epoxy-ceramic coatings, ARC MX1 was the most difficult to be applied since the mixed compound was very thick and dense. The number of hard ceramic particles was obviously adjusted so that the portion of carbides is as high as possible. Moreover, it seemed that ARC MX1 left easily voids or pores inside the final coating.

REFERENCES

A&A Coatings. 2016. Understanding Metal Alloy Coatings. Available: https://www.thermal-spray.com/understanding-metal-alloy-coatings/. Accessed 15 April 2020.

Abdelbary, A. 2014. Wear of Polymers and Composites. Cambridge: Woodhead Publishing.

Agarwal, T., Chaudhary, S. & Verma, S. 2016. Numerical and experimental analysis of silt erosion in pump as turbine (PAT). International Journal of Mechanical and Production Engineering Research and Development, 47-60.

Ahmedizat, S.R., Al-Zubaidi, A.B., Al-Tabbakh, A.A., Achour, A. & Hamead, A.A. 2019. Comparative study of erosion wear of glass fiber/epoxy composite reinforced with Al_2O_3 nano and micro particle. Materials Today: Proceedings 20(4), 420-427.

All Pumps. 2020. Industrial pumps. Available: https://allpumps.com.au/industrial-pumps/. Accessed 05 February 2020.

Araldite specification. Araldite AW4858 / HW4858. Huntsman Advanced Materials.

Arani, H., Rabba, W. & Papini, M. 2019. Solid particle erosion of epoxy matrix composites reinforced by Al_2O_3 spheres. Tribology International 136, 432-445.

ASTM G40-02. 2002. Standard Terminology Relating to Wear and Erosion. West Conshohocken: ASTM International.

Belzona. 2014. How an epoxy coating prolonged pump life. World pumps 2014(4), 16-17.

Belzona. 2015. Beating abrasive challenges keeps the ore flowing. World pumps 2015(6), 20-22.

Belzona. 2017. Erosion, corrosion & chemical attack. World pumps 2017(2), 20.

Belzona. 2018. Polymeric coatings extend pump lifespan. World pumps 2018(5), 34-35.

Belzona. 2019. Polymeric solutions for pump efficiency improvement: The Cost-Effective Approach to Maintaining Fluid Flow. Available: https://www.belzona.com/assets/data/literature/brochures/en/cat-pump-efficiency-en.pdf. Accessed 17 April 2020.

Belzona. 2020. Products: Belzona 1811 (Ceramic Carbide). Available: https://www.belzona.com/en/products/1000/1811.aspx. Accessed 03 March 2020.

Belzona. Know-how in action 11, No 21. Belzona 1811 keeps the mills working.

Belzona. Know-how in action 23, No 76. Belzona protects pipe elbows from abrasion.

Belzona. Know-how in action 26, No 36. Belzona protects pipeline and valves from cement abrasion.

Belzona. Know-how in action 28, No 126. Belzona 1811 ceramic carbide extends life of pump casing.

Belzona. Know-how in action 32, No 11. Belzona abrasion resistant lining for de-barker.

Belzona. Product Flyer: Belzona 1811 – Industrial Paste-Grade Lining for Protection Against Abrasive Attack.

Belzona. Product Flyer: Belzona 2121 – Durable & Abrasion resistant elastomer.

Belzona. Product specification sheet: Belzona 1811.

Budinski, K.G. 2007. Guide to Friction, Wear, and Erosion Testing. West Conshohocken: ASTM International.

Centria University of Applied Sciences. 2020. Research and Development. Project: CINEMA - Towards circular economy via eco-design and sustainable remanufacturing. Available: https://tki.centria.fi/hanke/cinema/1656. Accessed 25 March 2020.

Chang, B.P. & Hazizan, M.A. 2013. Comparative study of micro-and nano-ZnO reinforced UHMWPE composites under dry sliding wear. Wear 297, 1–2.

Chesterton. ARC Efficiency & Protective coatings. Product Datasheet: ARC MX1.

Chesterton. ARC Efficiency & Protective coatings. Product Datasheet: ARC BX2.

Chesterton. Case Study 015. FGD Recirculating Slurry Pump – ARC MX1, BX2, S2 and 855 Coatings.

Chesterton. Case Study 084. Thickener feed pump – ARC MX1 coating.

Chesterton. Case Study 104. Limestone slurry recirculation pumps – ARC BX2 and MX1 Coatings.

Chesterton. Case Study 111. Split case slurry pump – ARC MX1 & 855 Coatings.

Chesterton. Case Study 115. Tech-Taylor Isolation Valve – ARC MX1 Coating.

Chesterton. Case Study 128. Limestone slurry pump seal adapter plate – ARC MX1 coating.

Cinar, K., Ozmen Eruslu, S., Savas Dalmis, I. & Guven, I. 2019. Effect of particle shape on the wear and friction behavior of particle-reinforced epoxy coatings. Journal of Coatings Technology and Research 16, 1435–1445.

Davis, J.R. 2001. Surface engineering for corrosion and wear resistance. Russell Township: Materials Park, ASM International.

DeFelsko. 2020. Full guide v. 5.0. – PosiTest AT Series Pull-Off Adhesion Testers.

DeFelsko. 2011. YouTube: PosiTest AT-A - Automatic Adhesion Tester. Available: https://www.youtube.com/watch?v=N92ryobkPvA. Accessed 11 December 2019.

Devaprakasam, D., Hatton, P.V., Möbus, G. & Inkson, B.J. 2008. Effect of microstructure of nano- and micro-particle filled polymer composites on their tribo-mechanical performance. Journal of Physics: Conference Series 126 (1), 012057.

Durand, J.M., Vardavoulias, M. & Jeandin, M. 1995. Role of reinforcing ceramic particles in the wear behaviour of polymer-based model composites. Wear 182-183(2), 833-839.

Ebnesajjad, S. 2014. Surface Treatment of Materials for Adhesive Bonding. Norwich: William Andrew Publishing.

Fengkun, L., Yuqin, Y., Shuqin, L., Dongbo, W., Shiyuan, W., Feng, D., Baozhang, D., Zhangzhong, W. & Pingze, Z. 2019. Wear resistance of Al_2O_3/WC-Co/epoxy coatings on TC18 (Ti-5Al-5Mo-5V-1Cr-1Fe) alloy. Surface & Coatings Technology 374, 1100-1107.

Friedrich, K. 2018. Polymer composites for tribological applications. Advanced Industrial and Engineering Polymer Research 1(1), 3-39.

Gilbert, N. 2012. Structural Steel - S235, S275, S355 Chemical Composition, Mechanical Properties and Common Applications. Available: https://www.azom.com/article.aspx?ArticleID=6022. Accessed 04 March 2020.

Holmberg, K. & Erdemir, A. 2017. Influence of tribology on global energy consumption, costs and emissions. Friction 5(3), 263–284.

Improve Engineering System. Products: Tungsten Carbide / Nickel Chrome Coating. Available: http://www.improveengineer.com/carbide-coating.html. Accessed 16 April 2020.

Inamuddin, I., Boddula, R., Ahamed, M.I. & Asiri, A.M. 2020. Polymers Coatings: Technology and Applications. Beverly: Scrivener Publishing LLC.

Jia, X. & Ling, X. 2005. Influence of Al_2O_3 reinforcement on the abrasive wear characteristic of Al_2O_3/PA1010 composite coatings. Wear 258, 1342–1347.

Kandeva, M., Vencl, A. & Karastoyanov, D. 2016. Advanced Tribological Coatings for Heavy-Duty Applications: Case Studies. Sofia: Institute of Information and Communication Technologies, Bulgarian Academy of Sciences.

Kato, K. & Adachi, K. 2000. Modern Tribology Handbook Volume 1, Chapter 7: Wear mechanisms. Boca Raton: CRC Press LLC.

Kopeliovich, D. 2020. SubsTech: Mechanisms of wear. Available: http://www.substech.com/dokuwiki/doku.php?id=mechanisms_of_wear&s=mechanism. Accessed 05 April 2020.

L&L Special Furnace. 2018. What are ceramic matrix composites? Available: https://llfurnace.com/blog/what-are-ceramic-matrix-composites/. Accessed 16 April 2020.

Li, S. 2015. Intelligent Coatings for Corrosion Control: Chapter 20 – Monitoring Corrosion Using Vibrational Spectroscopic Techniques. Oxford: Butterworth-Heinemann.

Mai, Y.-W. & Yu, Z.-Z. 2006. Polymer nanocomposites. Cambridge: Woodhead Publishing.

Maier, P. & King, C. 2009. Energy savings through pump refurbishment and coating. New York: The New York state energy research and development authority.

Nashett, R. & Lyman, J. A. (Henkel). 2015. Wear resistance ceramic coatings. Available: https://www.plantengineering.com/articles/wear-resistant-ceramic-coatings/. Accessed 11.02.2020

Näkki, J. 2019. R&D Specialist at Centria University of Applied Sciences. Document: Epoxy-ceramic composite coatings, research plan.

Oliveira, J.D., Rocha, R.C. & Galdino, A.G. 2019. Effect of Al_2O_3 particles on the adhesion, wear, and corrosion performance of epoxy coatings for protection of umbilical cables accessories for subsea oil and gas production systems. Journal of materials research and technology 8(2), 1729-1736.

Ojala, N., Kuokkala, V.-T., Valtonen, K., Kivikytö-Reponen, P. & Vuorinen, P. 2012. High speed slurry-pot type erosion wear tester. The 15th Nordic Symposium on Tribology-NordTrib2012, 1-6.

Ojala, N. 2017. Application oriented wear testing of wear resistant steels in mining industry. Tampere: Tampere University of Technology. Doctoral thesis.

Ojala, N., Valtonen, K., Minkkinen, J. & Kuokkala, V.-T. 2017. Edge and particle embedment effects in low- and high-stress slurry erosion wear of steels and elastomers. Wear 388–389, 126–135.

Palraj, S., Meena, K., Maruthan, K. & Rajagopal, G. 2015. Corrosion and wear resistance behavior of nano-silica epoxy composite coatings. Progress in Organic Coatings 81, 132-139.

Pape, P.G. 2011. Applied Plastics Engineering Handbook - Processing and Materials. Chapter 28: Adhesion Promoters: Silane Coupling Agents. Oxford: William Andrew.

Park, S.-J. & Seo, M.-K. 2011. Interface Science and Composites. Interface Science and Technology 18. Amsterdam: Academic Press.

Patnaik, A., Satapathy, A. & Mahapatra, S.S. 2007. Implementation of Taguchi method for tribo-performance of hybrid composites. Proceedings of the Eighth International Conference on Operations and Quantitative Management, 779-789. Bangkok: Assumption University.

Penticton Foundry. 2017. The Differences Between Ni-Hard and Chrome White Iron. Available: https://www.pentictonfoundry.com/news/differences-between-ni-hard-and-chrome-white-iron/. Accessed 05 March 2020.

Precision Coatings Inc. Ceramic Coatings. Available: http://www.precisioncoatings.com/ceramic-coatings/. Accessed 15 April 2020.

RAEX. 2020. Raex - Any time, any wear.

Ruzga, R., Willis, P. & Kumar, A. 1993. USACERL Technical Report FM-93/0, Application of Thermal Spray and Ceramic Coatings and Reinforced Epoxy for Cavitation Damage Repair of Hydroelectric Turbines and Pumps. Champaign: U.S. Army Construction Engineering Research Laboratories.

Schramm, B., Dwars, A. & Kühl, A. 2005. Do coatings protect against corrosion and wear? World pumps. World Pumps 470, 32-38.

SFS-EN 12513. Founding – Abrasion resistant cast irons. 2011. Helsinki: Finnish Standard Association SFS.

Smith, P. & Kraenzler, T. 2017. Reducing effects of corrosion and erosion. World Pumps (2), 38-41.

Sokol, M. 2019. What is a Polymer Coating? Available: https://www.adv-polymer.com/blog/polymer-coating. Accessed 16 April 2020.

SSAB. 2017. Raex 400. Datasheet. Available: https://www.raexsteel.fi/api/sitecore/Datasheet/GetDocument?productId=8FF3B7C14D6944A2BCF323ECF99088BC&language=en. Accessed 15 May 2020.

Stachowiak, G.W. & Batchelor, A.W. 1993. Engineering Tribology. Amsterdam: Elsevier Science Publishers B.V.

Symonds, N. & Mellor, B.G. 1999. Polymeric coatings for impact and wear resistance I: Wear. Wear 225–229(1), 111–118.

Taber Industries. 2020. Genuine Taber Abrading Wheels. Available: https://www.taberindustries.com/taber-abrading-wheels. Accessed 15 March 2020.

Taber Industries. 2020. Taber rotary abraser. Available: https://www.taberindustries.com/taber-rotary-abraser. Accessed 15 March 2020.

Tampere Wear Center (TWC). 2019. Research equipment. Tampere: Tampere University.

Verosky, K., Maier, P., White, R., Connell, S., Knoll, K., King, C., Hanley, G. & Metzger, R. 2008. Energy Savings through Pump Refurbishment and Coatings. Pumps & Systems. Available: https://www.pumpsandsystems.com/energy-savings-through-pump-refurbishment-and-coatings. Accessed 21 February 2020.

Vijay, P.V., Soti, P.R., Banerjee, D.A. & Sierros, K.A. 2019. Abrasion resistance of polymer and polymer–ceramic composite coatings for steel hydraulic structures. Journal of Coatings Technology and Research 17, 401–411.

Wang, Y.-F. & Yang, Z.-G. 2008. Finite element model of erosive wear on ductile and brittle materials. Wear 265(5-6), 871-878.

Wetzel, B., Haupert, F., Friedrich, K., Zhang, M.Q. & Rong, M.Z. 2001. Mechanical and tribological properties of microparticulate and nanopaticulate reinforced polymer composites. Proceedings of the 13th European Conference of Composite Materials.

Wu, J. & Cheng, X.H. 2006. The tribological properties of Kevlar pulp reinforced epoxy composites under dry sliding and water lubricated condition. Wear 261, 1293–1297.

Yan, H., Deng, Y., Su, Y.Y., Jiang, S., Chen, Q.W., Cao, S.X. & Liu, B. 2019. Ti(C, N)-Based Cermets with Two Kinds of Core-Rim Structures Constructed by β-Co Microspheres. Advances in Materials Science and Engineering, 1-11.

Zahavi, J. & Schmitt, J.F. 1981. Solid particle erosion of reinforced composite materials. Wear 71(2), 179-190.

Zhou, R., Lu, D.H., Jiang, Y.H. & Li, Q.N. 2005. Mechanical properties and erosion wear resistance of polyurethane matrix composites. Wear 259(1–6), 676-683.

Zum Gahr, K.H. 1987. Microstructure and Wear of Materials. Amsterdam: Elsevier Science Publishers B.V.